

REPORT DOCUMENTATION PAGE			Form Approved OMB NO. 0704-0188		
<p>The public reporting burden for this collection of information is estimated to average 1 hour per response, including the time for reviewing instructions, searching existing data sources, gathering and maintaining the data needed, and completing and reviewing the collection of information. Send comments regarding this burden estimate or any other aspect of this collection of information, including suggestions for reducing this burden, to Washington Headquarters Services, Directorate for Information Operations and Reports, 1215 Jefferson Davis Highway, Suite 1204, Arlington VA, 22202-4302. Respondents should be aware that notwithstanding any other provision of law, no person shall be subject to any penalty for failing to comply with a collection of information if it does not display a currently valid OMB control number.</p> <p>PLEASE DO NOT RETURN YOUR FORM TO THE ABOVE ADDRESS.</p>					
1. REPORT DATE (DD-MM-YYYY) 28-02-2012		2. REPORT TYPE Final Report		3. DATES COVERED (From - To) 15-May-2008 - 14-Nov-2011	
4. TITLE AND SUBTITLE Towards DNA-Based Programmable Matter: Final Report			5a. CONTRACT NUMBER W911NF-08-1-0151		
			5b. GRANT NUMBER		
			5c. PROGRAM ELEMENT NUMBER 8D10AN		
6. AUTHORS David Gorin, Yu He, Jia Niu, John Sadowski, David R. Liu			5d. PROJECT NUMBER		
			5e. TASK NUMBER		
			5f. WORK UNIT NUMBER		
7. PERFORMING ORGANIZATION NAMES AND ADDRESSES Harvard University Office of Sponsored Research 1350 Massachusetts Ave. Holyoke 727 Cambridge, MA 02138 -			8. PERFORMING ORGANIZATION REPORT NUMBER		
9. SPONSORING/MONITORING AGENCY NAME(S) AND ADDRESS(ES) U.S. Army Research Office P.O. Box 12211 Research Triangle Park, NC 27709-2211			10. SPONSOR/MONITOR'S ACRONYM(S) ARO		
			11. SPONSOR/MONITOR'S REPORT NUMBER(S) 54543-MS-DRP.3		
12. DISTRIBUTION AVAILABILITY STATEMENT Approved for Public Release; Distribution Unlimited					
13. SUPPLEMENTARY NOTES The views, opinions and/or findings contained in this report are those of the author(s) and should not be construed as an official Department of the Army position, policy or decision, unless so designated by other documentation.					
14. ABSTRACT We completed a series of pilot studies towards the development of DNA-programmed mesoscale and nanoscale materials. We developed a computational and experimental infrastructure that enabled the translation of arbitrary three-dimensional models into DNA sequences that encode their assembly. We developed a suite of surface chemistries to functionalize a variety of mesoscale materials with DNA oligonucleotides. Finally, we demonstrated the ability of these DNA-linked surfaces to mediate surface-surface interactions in a DNA sequence-specific					
15. SUBJECT TERMS DNA, mesoscale materials, DNA hybridization, programmable matter					
16. SECURITY CLASSIFICATION OF:			17. LIMITATION OF ABSTRACT UU	15. NUMBER OF PAGES	19a. NAME OF RESPONSIBLE PERSON David Liu
a. REPORT UU	b. ABSTRACT UU	c. THIS PAGE UU			19b. TELEPHONE NUMBER 617-496-1067

Report Title

Towards DNA-Based Programmable Matter: Final Report

ABSTRACT

We completed a series of pilot studies towards the development of DNA-programmed mesoscale and nanoscale materials. We developed a computational and experimental infrastructure that enabled the translation of arbitrary three-dimensional models into DNA sequences that encode their assembly. We developed a suite of surface chemistries to functionalize a variety of mesoscale materials with DNA oligonucleotides. Finally, we demonstrated the ability of these DNA-linked surfaces to mediate surface-surface interactions in a DNA sequence-specific manner. In a second line of research, we applied these principles to create higher-order nanometer-scale plasmonic structures from DNA-linked gold nanospheres and nanoshells.

Enter List of papers submitted or published that acknowledge ARO support from the start of the project to the date of this printing. List the papers, including journal references, in the following categories:

(a) Papers published in peer-reviewed journals (N/A for none)

Received

Paper

08/15/2011	2.00	Yu He, David R. Liu. A Sequential Strand-Displacement Strategy Enables Efficient Six-Step DNA-Templated Synthesis, Journal of the American Chemical Society, (07 2011): 9972. doi: 10.1021/ja201361t
------------	------	--

TOTAL: 1

Number of Papers published in peer-reviewed journals:

(b) Papers published in non-peer-reviewed journals (N/A for none)

Received

Paper

TOTAL:

Number of Papers published in non peer-reviewed journals:

(c) Presentations

Presented research strategy and results at three DARPA Programmable Matter meetings.

Number of Presentations: 3.00

Non Peer-Reviewed Conference Proceeding publications (other than abstracts):

<u>Received</u>	<u>Paper</u>
-----------------	--------------

TOTAL:

Number of Non Peer-Reviewed Conference Proceeding publications (other than abstracts):

Peer-Reviewed Conference Proceeding publications (other than abstracts):

<u>Received</u>	<u>Paper</u>
-----------------	--------------

TOTAL:

Number of Peer-Reviewed Conference Proceeding publications (other than abstracts):

(d) Manuscripts

<u>Received</u>	<u>Paper</u>
-----------------	--------------

08/15/2011	1.00	Federico Capasso, David R. Liu, Jonathan A. Fan, Yu He, Kui Bao, Chihhui Wu, Jiming Bao, Nicholas B. Schade, Vinothan N. Manoharan, Gennady Shvets, Peter Nordlander. DNA Enabled Self-Assembly of Plasmonic Nanoclusters, (08 2011)
------------	------	--

TOTAL:	1
---------------	----------

Number of Manuscripts:

Books

<u>Received</u>	<u>Paper</u>
-----------------	--------------

TOTAL:

Patents Submitted

Patents Awarded

Awards

2008-9 Member of the Defense Sciences Study Group (DSSG)
2009 Joined the JASONs, academic advisors to the U. S. government on science and technology
2009 Thomas T. Hoopes prize shared with Meera Atreya for her outstanding Senior Thesis
2011 Former Liu Group graduate student Dr. Kevin Esvelt received a Harold W. Weintraub Graduate Student Award, a national honor to recognize outstanding achievement in graduate research
2011 Former Liu Group graduate student Dr. Kevin Esvelt received the Fannie and John Hertz Foundation Doctoral Thesis Prize to recognize “overall excellence and pertinence to high-impact applications of the physical sciences”

Graduate Students

<u>NAME</u>	<u>PERCENT SUPPORTED</u>	Discipline
John Sadowski	1.00	
Jia Niu	0.50	
FTE Equivalent:	1.50	
Total Number:	2	

Names of Post Doctorates

<u>NAME</u>	<u>PERCENT SUPPORTED</u>
David Gorin	0.50
Yu He	1.00
FTE Equivalent:	1.50
Total Number:	2

Names of Faculty Supported

<u>NAME</u>	<u>PERCENT SUPPORTED</u>	National Academy Member
David R. Liu	0.00	
FTE Equivalent:	0.00	
Total Number:	1	

Names of Under Graduate students supported

<u>NAME</u>	<u>PERCENT SUPPORTED</u>
FTE Equivalent:	
Total Number:	

Student Metrics

This section only applies to graduating undergraduates supported by this agreement in this reporting period

The number of undergraduates funded by this agreement who graduated during this period: 0.00

The number of undergraduates funded by this agreement who graduated during this period with a degree in science, mathematics, engineering, or technology fields:..... 0.00

The number of undergraduates funded by your agreement who graduated during this period and will continue to pursue a graduate or Ph.D. degree in science, mathematics, engineering, or technology fields:..... 0.00

Number of graduating undergraduates who achieved a 3.5 GPA to 4.0 (4.0 max scale): 0.00

Number of graduating undergraduates funded by a DoD funded Center of Excellence grant for Education, Research and Engineering:..... 0.00

The number of undergraduates funded by your agreement who graduated during this period and intend to work for the Department of Defense 0.00

The number of undergraduates funded by your agreement who graduated during this period and will receive scholarships or fellowships for further studies in science, mathematics, engineering or technology fields: 0.00

Names of Personnel receiving masters degrees

NAME

Total Number:

Names of personnel receiving PHDs

NAME

Total Number:

Names of other research staff

NAME

Aleks Markovic

FTE Equivalent:

Total Number:

PERCENT SUPPORTED

0.09

0.09

1

Sub Contractors (DD882)

Inventions (DD882)

Scientific Progress

Please see the attached documents.

Technology Transfer

Programmable Matter Final Report

Liu Team (Harvard)

Project overview

We propose the development and initial implementation of programmable matter, a new concept in materials. Programmable matter is constructed of mesoscale (mm-cm) building blocks that undergo self-assembly when exposed to a set of instructions specifying a desired three-dimensional target structure. When the target structure is no longer needed, the user can induce its efficient disassembly into building blocks that are suitable for future reassembly.

To realize this ambitious concept, we propose the creation of polyhedral mesoscale building blocks (“smartblocks”) that are densely functionalized with DNA oligonucleotides on their surfaces. Each face of each smartblock is linked to many copies of a unique oligonucleotide, such that no two smartblock faces display the same DNA sequence. To induce the programmable assembly of these smartblocks into target structures, we propose to use “megastaples,” long DNA duplexes terminated in single-stranded regions that are complementary to the oligonucleotides attached to two smartblock faces. Each megastaple therefore mediates the association of one pair of smartblocks via one smartblock-megastaple-smartblock interface, and a set of megastaples in principle can program the self-assembly of any stable three-dimensional structure. (Figure 1)

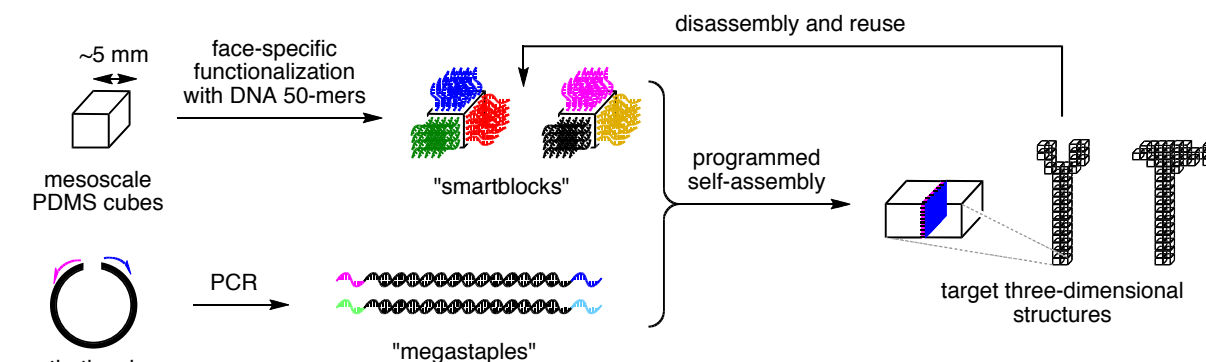


Figure 1

The successful creation of programmable matter will require the development and integration of a number of concepts— some unprecedented— in computer science, chemistry, and materials science. We previously developed a framework for the development of these concepts in the form of three Tasks comprising nine Milestones. The Milestones for Phase I and Phase II are as follows:

Milestone 1a: Develop a computational algorithm that outputs sets of hundreds to thousands of orthogonal ~50-base DNA sequences suitable for linkage to mesoscale polyhedra and suitable for the termini of megastaples.

Milestone 1b: Develop a software interface that accepts standard representations of three-dimensional structures together with a set of smartblock sequences and outputs a list of megastaple sequences suitable for mediating the self-assembly of the structure.

Milestone 2a: Prepare and characterize a variety of candidate surfaces covalently linked to DNA strands of varying composition and linkage chemistries.

Milestone 2b: Develop a format for megastaples, experimentally validate the principle of DNA base pairing-mediated mesoscale surface assembly, and measure the interaction strengths afforded by such an approach.

Summary of Progress:

We have already achieved all three of the Phase I milestones listed above. We have developed and implemented an optimized algorithm that outputs hundreds to thousands of DNA 50-mer sequences that satisfy the orthogonality requirements that will be essential for our vision of programmable matter. We have also developed an interface with Visual OMP, an advanced commercially available oligonucleotide modeling platform, that enables the rapid screening of these algorithmically generated sequences to eliminate high melting-temperature spurious interaction. The generation, modeling, and screening of DNA sequences suitable for our early experimental efforts represent crucial capabilities that are now in hand (Milestone 1a).

We also implemented in the form of a separate software program the ability to input a standard three-dimensional representation of an object (in the form of an AutoCAD file) and rasterize that object into smartblocks of arbitrary shape. We have tested this ability using basic shapes such as spheres, as well as more sophisticated arbitrary shapes such as wrenches. We are initially focusing our efforts on two smartblock shapes: cubes and truncated octahedrons. We believe these two smartblocks represent an attractive balance between ease of preparation and ease of self-assembly.

We have also developed and tested a variety of surface functionalization chemistries that enable the covalent attachment of DNA to glass and PDMS surfaces. We implemented the most promising of these chemistries and measured the functionalization density on glass and PDMS surfaces as $\sim 10^{12}$ and $\sim 10^{13}$ DNA 50-mers per 0.25 cm^2 . Both functionalization densities are already well above our stated goal of at least 10^{11} DNA 50-mers per 0.25 cm^2 of surface.

In addition, we completed a portion of Milestone 2b during Phase I, by synthesizing and characterizing megastaples. We used a PCR-based method to synthesize the megastaples using primers attached to our handle sequences using an unnatural spacer. We then confirmed the structure of our megastaples through both gel electrophoresis, and a fluorescence binding assay. We also conducted extensive experiments on three different approaches to DNA hybridization-mediated surface-surface interaction. Most recently, we have embarked on a new approach to achieving DNA-mediated surface associations that uses extremely long, highly repetitive single-stranded DNAs linked to a variety of surfaces. This new approach in principle offers much more flexibility for productive DNA hybridization and potential interaction strength than our initial approach, and is currently being tested for its ability to mediate detectable sequence-specific surface interactions.

We made substantial Phase II progress as well. Specifically, we used surface chemistries described below to generate DNA-linked glass and PDMS surfaces, and demonstrated surface-surface association that is dependent on DNA sequence, DNA structure, and DNA hybridization. Finally, we also applied these principles to the assembly of DNA-programmed plasmonic nanoclusters of gold spheres and gold shells functionalized the DNA oligonucleotides.

Milestone 1a: Sequence generation

Overview

J-Seqgen is software which generates a series of DNA sequences which are orthogonal to each other, i.e., they should not form complexes with each other above a certain threshold temperature. The input parameters are: strand length, number of strands, criterion length, and threshold temperature. The program also has the ability to preload sequences to be avoided during the main sequence generation. The program can output a human-readable text file and/or an OMP-compatible file containing the sequences.

The program generates the sequence using sequence symmetry minimization (SSM), and then optionally checks the melting temperatures using the commercial software Oligonucleotide Modeling Platform Developer Edition (OMP) from DNA Software.

Background

Sequence symmetry minimization:

SSM is a heuristic method that designs a sequence with no unintentional spurious interactions of a specified length. The essence of SSM is that, if a subsequence of a certain length appears in the sequence, its complement should not appear anywhere in any of the sequences that it is not designed to complex with. The subsequence length used in imposing this requirement is called the *criterion length* and each subsequence of this length is a *word*. Sequences which fulfill SSM will have no spurious complementary runs of at least the criterion length in any frame. For example, if the criterion length is 7, there will be no possibility of forming spurious duplexes of 7 or more bases.

Using a lower criterion length lowers the strength of undesired interactions; however, the size of the sequence set to be generated places a lower limit on the criterion length. For criterion length c there are only 4^c words available to be used. In our system, with m strands of length n plus their antistrands, the total number of words contained in a single strand is $n-c+1$, and the number of words contained in the whole system is $2m(n-c+1)$. Furthermore, the user may wish to exclude certain words such as those contained in the megastaple template. Since each word must be unique, c must be chosen so that $4^c - p \geq 2m(n-c+1)$, if p words are excluded.

Oligonucleotide modeling platform:

OMP is commercial software which calculates thermodynamic parameters such as the free energy change of hybridization (ΔG) and the melting temperature (T_m) for collections of strands. J-Seqgen interacts with OMP through the functionality provided in the Developer Edition of the software.

The algorithm

Pseudocode:

Preload excluded sequences into word hashtable.

For each strand:

Find an unused word to start the sequence.

While unassigned bases remain:

 Check whether adding each of the four bases is allowed.

If no base is allowed, back up one base.

Otherwise pick a random base from those allowed, advance to next base.

Once a candidate strand is generated, use OMP to **check** T_m of all heterodimers with previously generated strands; reject and regenerate if any T_m 's are greater than user-defined threshold.

Detailed explanation:

J-Seqgen uses a hashtable to store whether each of the 4^c possible words has been previously used and thus is unavailable to be used again. The advantage of a hashtable is that it can be accessed in constant time, which is vital for the linear scaling of the algorithm.

The program's user interface allows the user to preload words into the hashtable from a file, set the generation parameters (strand length, number of strands, criterion length, and melting temperature threshold), start the sequence generation, and output an OMP OEF file.

The sequence generation itself function starts by generating a random word to use as the first word in the strand; if this word has already been used, another random word is tried. Once an acceptable word is found, the program starts adding new bases one at a time. All four words generated by adding each of the four nucleotides are checked in the word hashtable. If a word has already been used, then that base is rejected. If all bases have been rejected, the loop backs up to the previous base. Otherwise, the algorithm randomly chooses one of the acceptable bases, and moves to the next base.

Once one complete strand sequence has been generated, the program then checks the candidate strand with OMP. It checks the pairwise melting temperature of the candidate strand with each of the previously generated strands, and considers the maximum of these. If this maximum melting temperature exceeds the user's threshold temperature, the algorithm rejects the strand, and generates a new one.

Running time:

The SSM algorithm runs in nearly linear time, since one extra word needs to be checked for each extra base to be generated. The algorithm deviates from linear time in that long sequences will back up more, but this is not observed to be significant unless the number of needed words is very close to the number of possible words for that criterion length ($4^c - p$).

OMP is observed to run in linear time with respect to the number of pairwise interactions. This gives an overall complexity of $O(m^2)$, where m is the number of strands. The complexity with respect to the strand length n has not been thoroughly examined but it seems to be much worse.

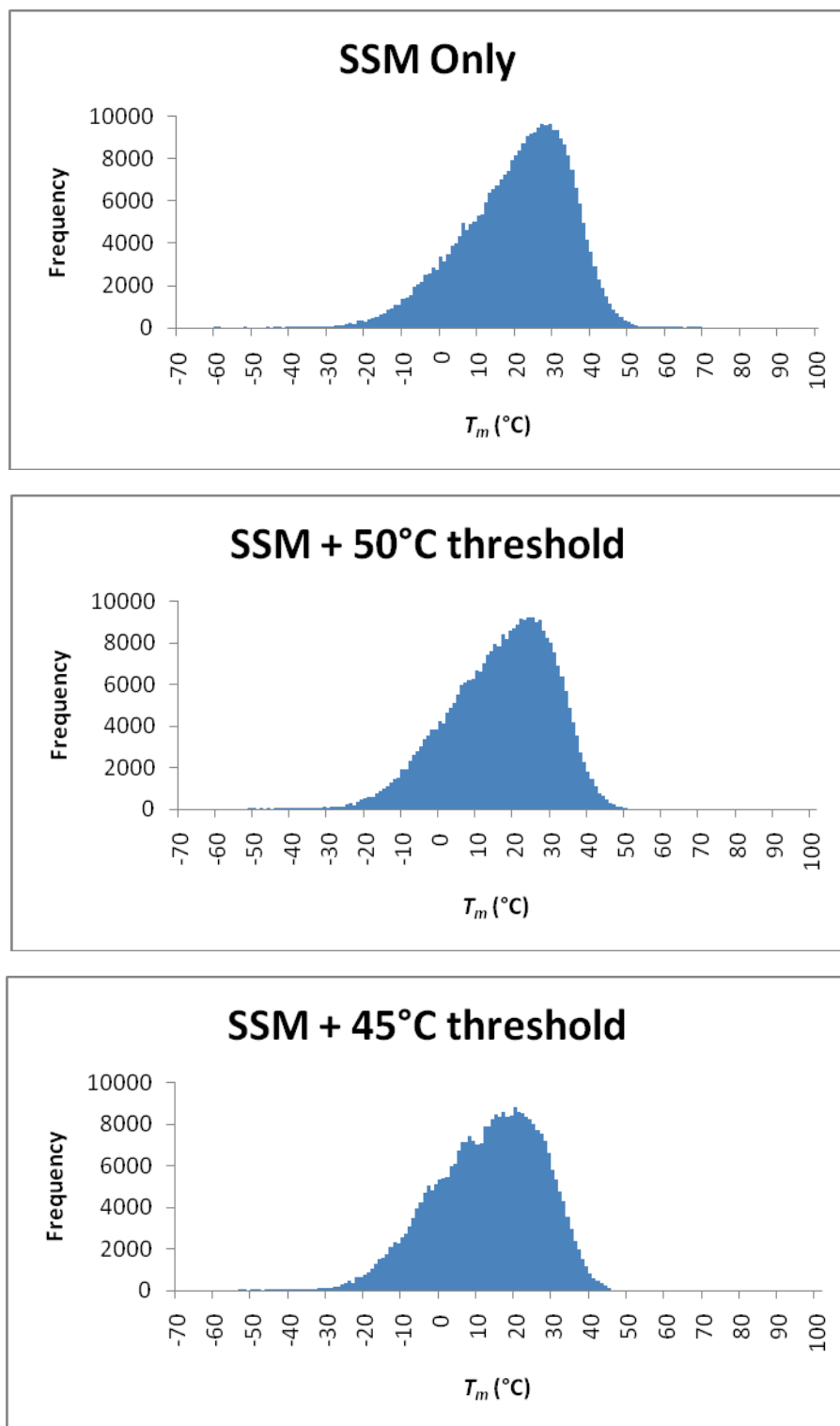


Figure 2. Histograms of the melting temperatures of pairwise spurious interactions in three different sets of 400 50-mers and their complements. The range for each data point in the histogram is 1 C°. *Top:* Sequence set generated using SSM only. *Middle:* Sequence set

generated using SSM, and using a threshold temperature of 50°C. *Bottom:* Sequence set generated using SSM, and using a threshold temperature of 45°C.

Overall, 1000 50-mers can be generated in <1 minute using only SSM. If OMP is used to check melting temperatures without rejecting any strands, the same generation will take ≈12 hours. Using a temperature threshold will increase the time needed since strand must be rejected and regenerated; a threshold temperature of 50°C will take ≈24 hours and a threshold temperature of 45°C will take nearly a week.

Results

Programming:

Melting temperature data for sets of 400 50-mers and their complements was generated (Figure 2). This comprises 800 strands total and 319,200 interactions. These were generated using sequence symmetry minimization (SSM) algorithm, both with no temperature threshold, and with checking by OMP using a threshold temperature of 50°C or 45°C.

Empirical confirmation:

Gel electrophoresis was performed (Figure 3) to demonstrate that duplexes only form between the intended sense and antisense handle strands generated by our software. Four sets of strands were arbitrarily chosen from our 1000-strand collection and incubated at 50°C in various combinations. Bands representing duplexes are visible in lanes where duplex formation is intended; no bands representing unintended interactions are observed in any lane in the gel.

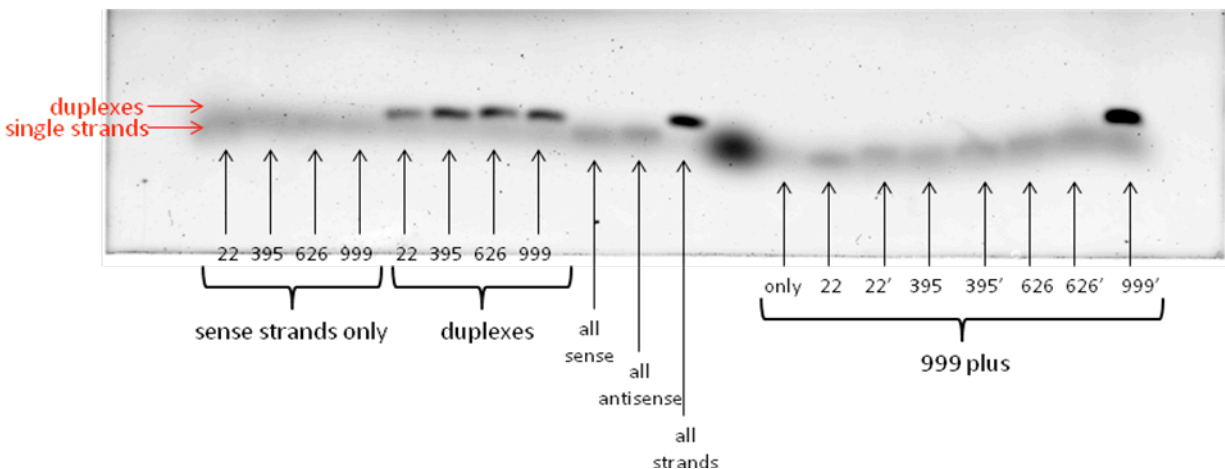


Figure 3. Gel electrophoresis of sequences. A prime symbol indicates the “antisense” complement of a strand. The left half of the gel shows single strands and duplexes, followed by combinations of all sense, all antisense, and all strands. The right half of the gel shows strand 999 plus each of the other strands; no interactions are observed except for the desired interaction with its complement. The experimental conditions were 1 pmol ea. strand in PBS buffer, incubated at 50°C for 1 hr, 2% agarose+EtBr, 100V, 25min.

Milestone 1b: Object rasterization

Overview

J-Honey is software which rasterizes an arbitrary shape into a set of polyhedra (smartblocks) which approximates it. It takes two inputs: the honeycomb lattice type, and a function which specifies whether a given set of coordinates is inside the desired shape. The output is a human-readable file containing the smartblock specifications, and/or an AutoCAD script representing the assembled smartblocks.

The smartblock specifications consist of, for each polyhedron, a polyhedron ID and the polyhedron type; and for each face, a sequence ID as well as the polyhedron ID of the complementary smartblock.

Background

A honeycomb lattices is a three-dimensional tessellation of solid polyhedra which completely fills space. There are 28 ways to fill space with convex uniform polyhedra:

cubic rectified cubic truncated cubic cantellated cubic bitruncated cubic cantitruncated cubic runcitruncated cubic omnitruncated cubic alternated cubic truncated alternated cubic runcinated alternated cubic cantitruncated alternated cubic quarter cubic gyrated alternated cubic	gyroelongated alternated cubic elongated alternated cubic gyrated triangular prismatic gyroelongated triangular prismatic truncated square prismatic snub square prismatic hexagonal prismatic truncated hexagonal prismatic trihexagonal prismatic triangular prismatic rhombi-trihexagonal prismatic omnitruncated trihexagonal prismatic snub trihexagonal prismatic elongated triangular prismatic
---	---

5 of these use only one type of polyhedron:

cubic: cubes

bitruncated cubic:
truncated octahedra

triangular prismatic:
triangular prisms

gyrated triangular prismatic:
triangular prisms

hexagonal prismatic:
hexagonal prisms

There are many other ways to fill space with a single type of non-uniform polyhedron. The program currently works with the **cubic** (cubes) and **bitruncated cubic** (truncated octahedra) honeycombs. It can be upgraded in future versions to work with more or custom honeycomb types.

The algorithm

Pseudocode:

Initialize: get honeycomb parameters from user

Create first polyhedron

For each face of current polyhedron

 Determine **coordinates** of adjacent polyhedron.

Query whether coordinates are **inside object**. If no, discard new polyhedron.

Query whether coordinates are **already occupied**. If yes, assign complimentary sequence ID's to corresponding faces.

Otherwise, create new polyhedron and place at end of queue.

Rerun for-loop on next shape in queue.

Detailed explanation:

The honeycomb type and a function describing the shape to be rasterized are set by the user. The JHoney object contains a queue of polyhedra stored in a linked list. The algorithm creates the first polyhedron at coordinates 0,0,0 and then considers each shape in the queue until it reaches the end. For each polyhedron, each face is considered individually in turn.

For a each face of a polyhedron, the algorithm first determines the coordinates of the polyhedron adjacent to the current face. It then determines whether this point is inside the object. If it is outside, the face is assigned to be an exterior face and the function returns, otherwise the function continues. The algorithm then checks if there is already a polyhedron at those coordinates. If yes, the sequence ID's of both complementary faces are set; if no, a new polyhedron is created with those coordinates (with the sequence ID's remaining unassigned), and placed at the end of the queue of polyhedra.

Once the algorithm is finished with one face, it runs subsequent faces on the same polyhedron, and eventually the program advances to the next shape in the queue, until the end of the queue is reached. Data can be output as either a human-readable text file or an AutoCAD script.

JHoney4ARX is additional code which allows the J-Honey software to be accessed from within the AutoCAD environment. It uses the ObjectARX for AutoCAD 2008 code library available from the Autodesk website. This code produces a file with a .arx extension. This file can be loaded into AutoCAD to activate the commands. JHoney4ARX allows the user to rasterize the object input into the AutoCAD program and output the human-readable or script file.

Results

Sample output is provided (Figure 4). Arbitrarily-shaped objects in AutoCAD can be rasterized into either cubes or truncated octahedra, along with the specifications for assigning DNA sequences to each of the smartblock faces.

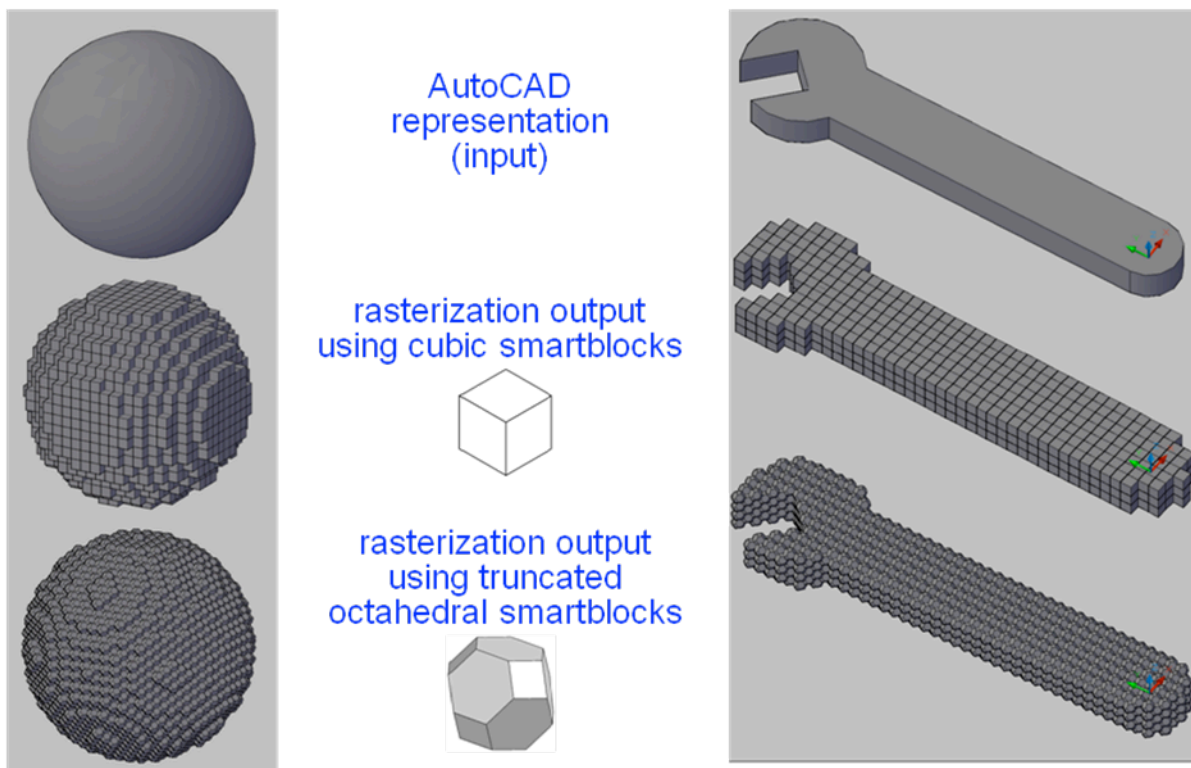


Figure 4. This demonstration of the Milestone 1b software shows an arbitrarily-shaped object rasterized into different honeycomb lattices. *Top:* the original objects, a sphere and a wrench. *Middle:* the objects as approximated by cubes. *Bottom:* the objects as approximated by truncated octahedra. This figure demonstrates both the success of our honeycombing algorithm as well as our ability to use an arbitrary, irregular shape from AutoCAD as an input. The honeycombing algorithm also generates a DNA sequence identifier for each face of each polyhedron, not shown.

Milestone 2a: Surface functionalization

Overview

Milestone 2a requires us to develop the surface chemistry needed to attach DNA oligonucleotides to a PDMS surface. We investigated a number of chemistries and characterized their suitability for DNA surface functionalization.

Results

PDMS oxidation:

The first step of surface functionalization is oxidation of the PDMS surface. Untreated PDMS surface is very hydrophobic. After plasma treatment, the surface becomes much more hydrophilic due to the formation of polar hydroxyl groups on the surface. We have found a good set of conditions at which we can obtain a hydrophilic PDMS surface (see Figure 5).

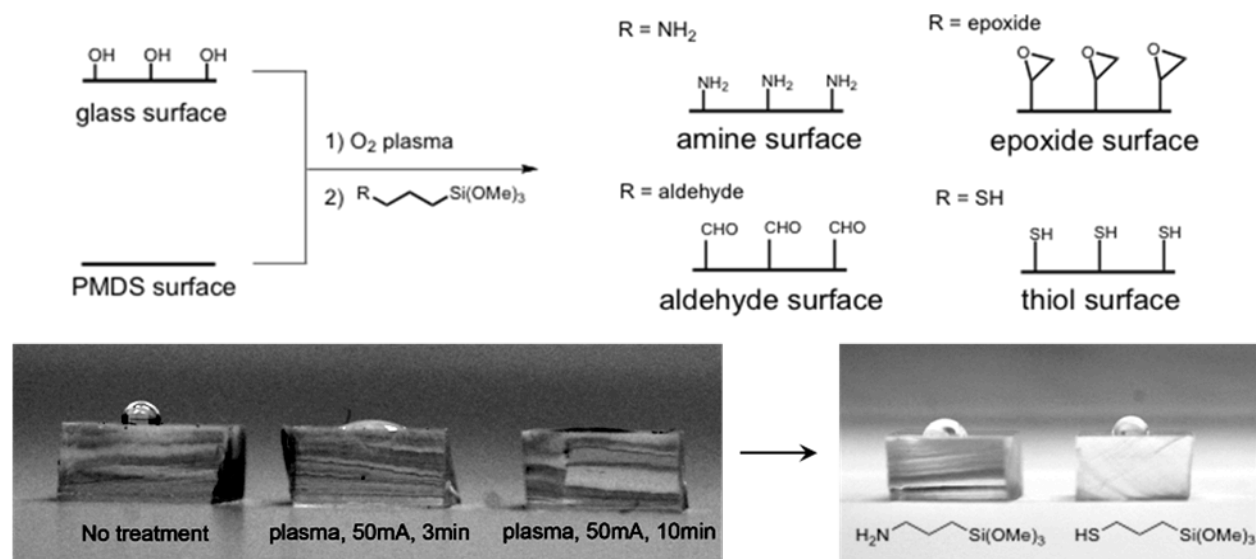
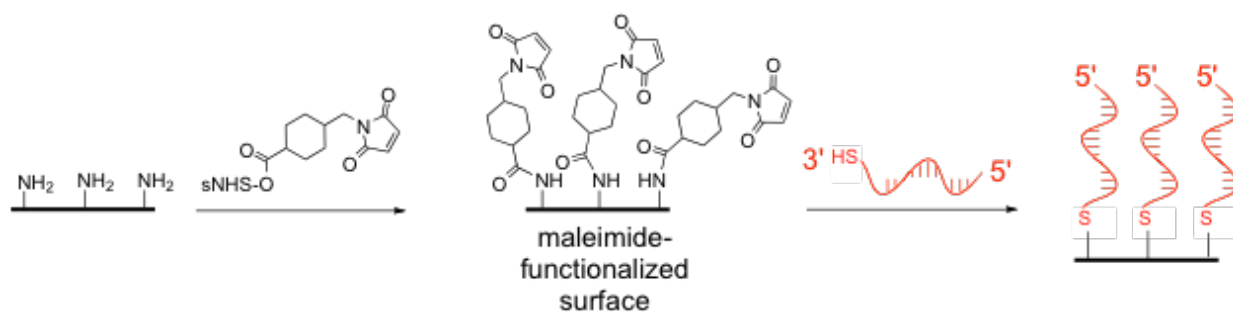


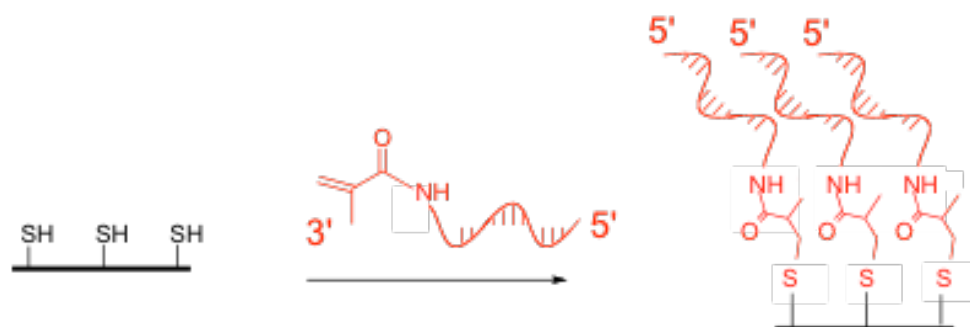
Figure 5. *Top:* The chemical scheme for chemically functionalizing glass and PDMS surfaces. *Bottom:* A 3 μ L water droplet on different PDMS surfaces. We can see that after a 50 mA, 10 min oxygen plasma treatment, the PDMS surface became rather hydrophilic and water easily spread out, which is the desired result. After silane deposition, the surface becomes hydrophobic again, as expected.

Coupling reactions:

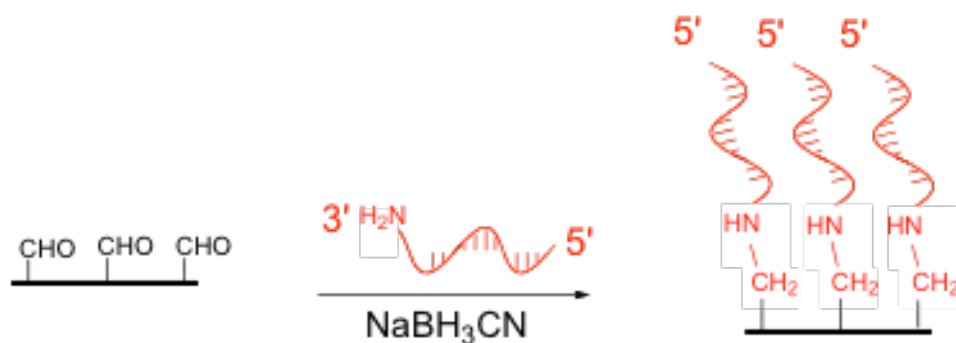
We tested four different DNA coupling reactions (Figure 6). The purpose of testing these reactions is to select the best one for the large-scale fabrication.



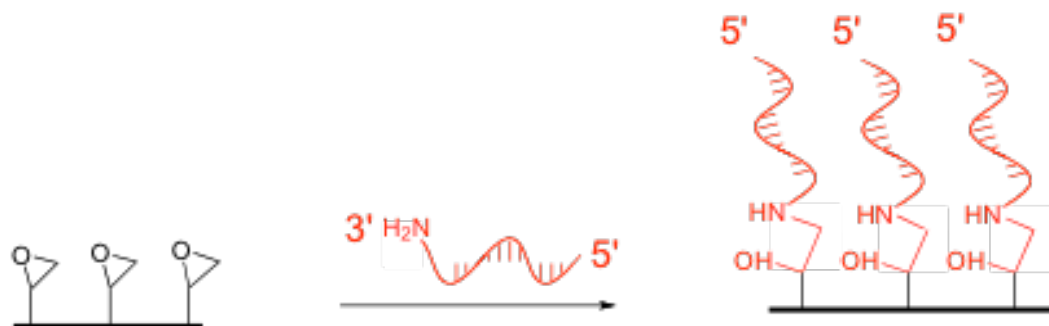
1) Amine surface to maleimide surface to DNA-linked surface via thiol-DNA



2) Thiol surface to DNA-linked surface via acrylamide-DNA



3) Aldehyde surface to DNA-linked surface via amine-DNA + NaCNBH_3



4) Epoxide surface to DNA-linked surface via amine-DNA

Figure 6. The four DNA coupling chemistries we considered.

The coupling efficiency was measured using a fluorescence assay. A fluorescently-labeled DNA oligomer was hybridized to the DNA immobilized on the surface, and the fluorescence was measured (Figure 7).

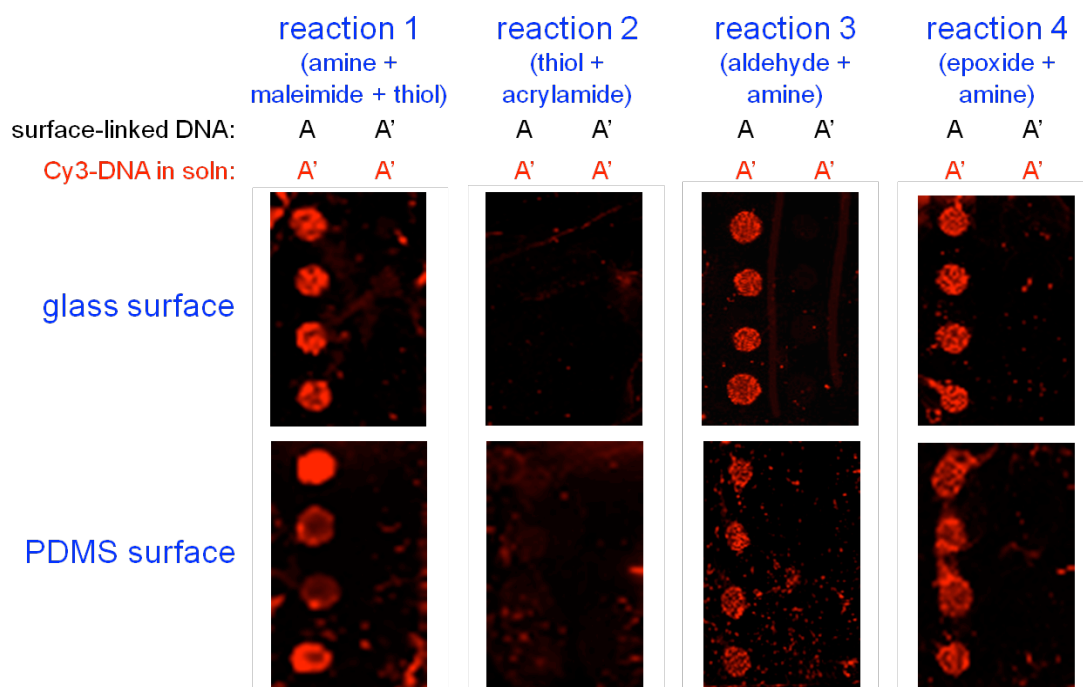


Figure 7. Fluorescence assay to evaluate the efficiency of the four coupling reactions we considered. In each of these images, the left column is the experiment and the right column is a negative control.

We selected the epoxide-amine reaction as the best candidate reaction based upon the coupling efficiency as well as its procedural simplicity and the availability of materials. Therefore, we decided to choose this reaction for all the following experiments.

An experiment was designed and carried out to quantitate the surface DNA density (Figure 8). We directly deposited different amounts of Cy3-labeled DNA on a substrate (either glass or PDMS), in order to create a working curve relating fluorescence intensity to fluorophore density. We then used this working curve to quantitate the density of a DNA-modified surface, after hybridization with Cy3-DNA, based on the fluorescence intensities.

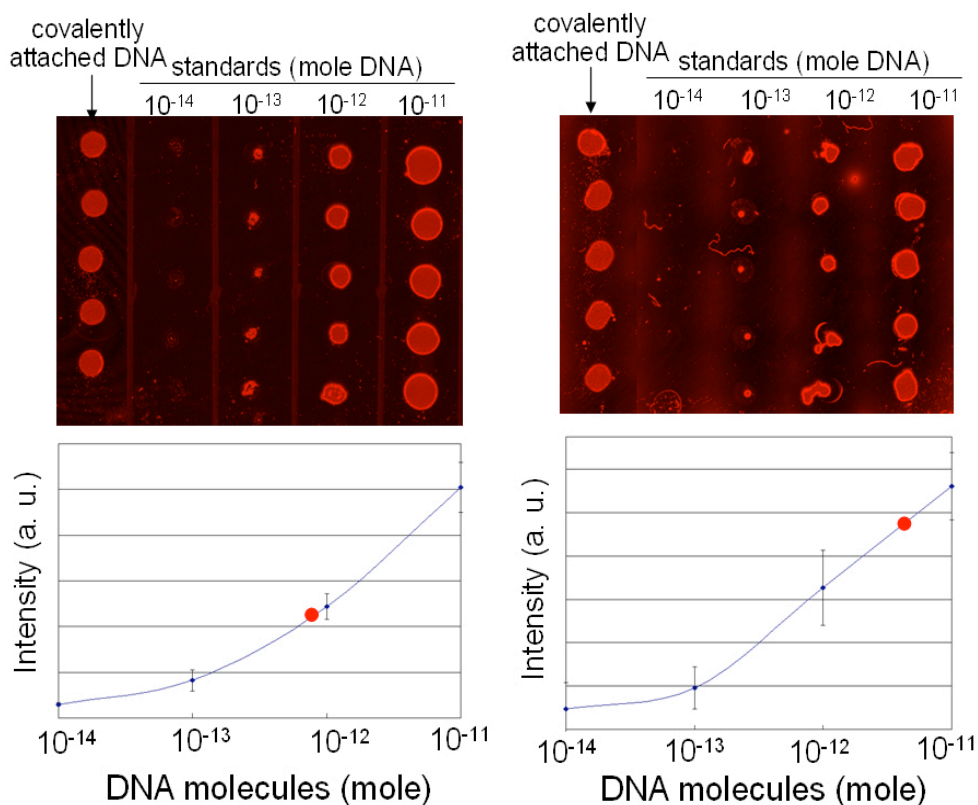


Figure 8. Covalently attached fluorescently-labeled DNA is compared to standards of known concentrations of free Cy3. *Left:* glass surface; *right:* PDMS surface. Plotting the DNA fluorescence on the standard curve yields DNA densities of 3.2×10^{12} and 3.3×10^{12} molecules/ 0.25 cm^2 respectively, surpassing our original goal.

These results indicate that we have achieved the goal (10^{11} molecules/ 0.25 cm^2) from our original proposal. Our DNA density after hybridization is greater than 10^{12} molecules/ 0.25 cm^2 .

Milestone 2d: Megastaple Synthesis

Overview

Milestone 2d requires us to develop a format for megastaples, which are about several thousands base pairs long DNA duplexes with two 50-mer single stranded overhangs on the both termini.

We have designed our megastaples as 2 kbp duplex DNA's with single-stranded overhangs complimentary to the smartblock handle oligonucleotides. This is for two reasons. First, the long duplex region will bridge micron-sized microscopic imperfections in the polyhedron surfaces (Figure 9). Second, it allows for all the assembly information to be encoded in the megastaples, so that different sets of megastaples will result in different controlled assemblies using the same smartblocks.

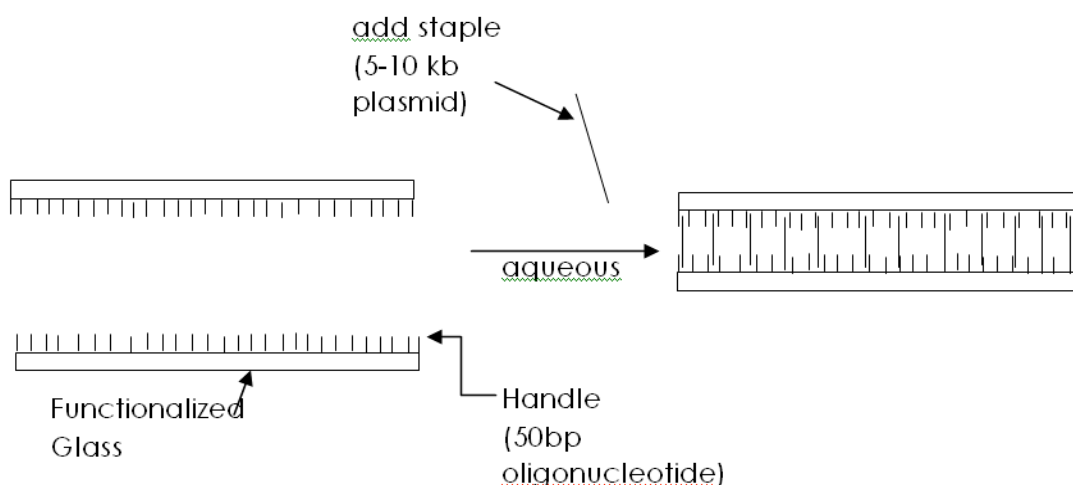


Figure 9. Schematic of the target Milestone 2b setup. Two surfaces are functionalized with oligonucleotide handles. Upon addition of megastaples containing overhangs complimentary to the surface handles, the two surfaces will adhere to each other. Addition of noncomplimentary megastaples would not result in adhesion, providing the selectivity vital for our proposed self-assembly method. Additionally, the length of the megastaples would allow them to bridge micron-scale imperfections in the surfaces.

Experimental design

We have used a polymerase chain reaction (PCR)-based method to synthesize megastaples. Our method is similar to standard PCR using a plasmid as a template, except that we use special primers which are connected to our handles via an organic spacer. The spacer blocks the polymerase from acting on the handle portion of the primer complex, which results in double-stranded megastaples with the handles remaining as single-stranded overhangs. This allows us to efficiently create the megastaple's duplex portion while retaining full control over the handle sequences.

It is critical that the handle regions of the megastaples remain single-stranded, since these comprise the sticky ends that will interface with the smartblock handles. We can confirm that the single-stranded regions exist through their ability to bind fluorescently-labeled oligonucleotides which are the compliments of our handle sequence (Figure 10). If the megastaple has the proper structure, it

should become fluorescent once annealed to the handle compliments, which can be confirmed by gel electrophoresis.

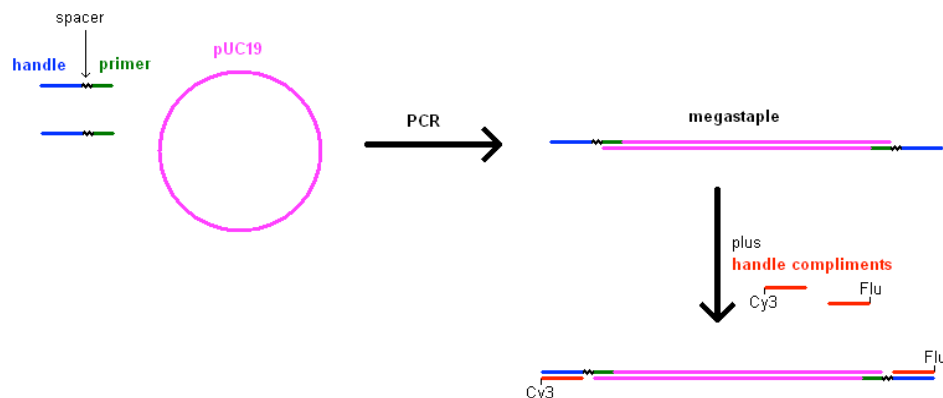


Figure 10. Scheme for synthesis and structure confirmation of megastaples. A polymerase chain reaction (PCR) is performed using special primers which are connected to our handles via an organic spacer, blocking the polymerase from acting on the handle region. The existence of the single-stranded handle regions can be experimentally determined by annealing the megastaples with the fluorescently-labeled handle compliments, and performing gel electrophoresis to determine megastaple fluorescence.

Results

We have verified the structure of the new megastaples by performing the fluorescence hybridization experiment explained above. The megastaple is clearly labeled by both handle compliments, meaning that sticky ends are available for smartblock hybridization. (Figure 11)

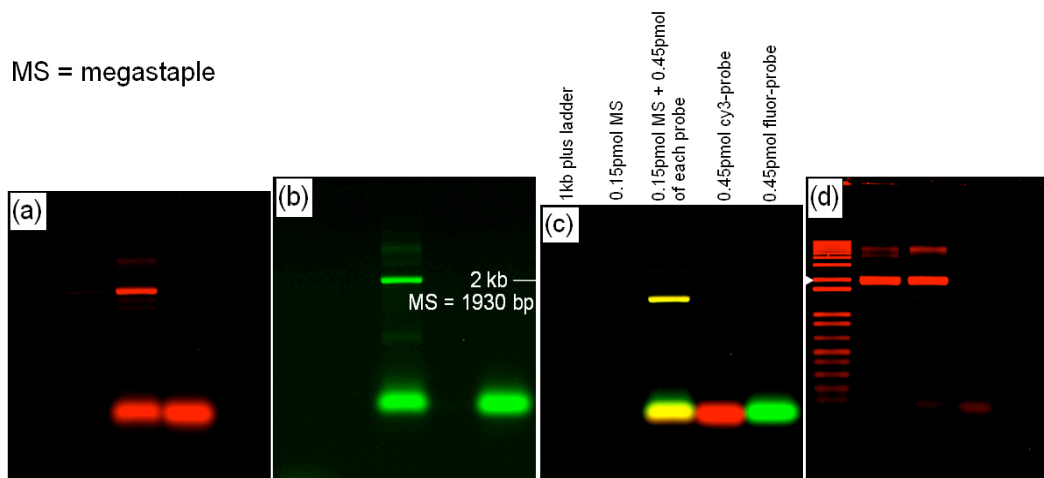


Figure 11. Images of a gel electrophoresis analysis of the fluorescently-labeled megastaple structure in Figure 10. *a*: Cy3 fluorescence. *b*: Fluorescein fluorescence *c*: Overlay of Cy3 and fluorescein fluorescence. *d*: Fluorescence after staining with ethidium bromide. The gel conditions are: 1% agarose, 100 V, 28 min. The lane labels over image c are valid for all images.

Based on a similar strategy, megastaples with length up to 8k base pairs were also successfully synthesized. The reason to develop longer megastaples is that surface defect is one of the major problems that inhibit DNA-mediated surface interaction. The 8k base pairs megastaples are expected to be able to tolerate surface defects up to $\sim 2.5\mu\text{m}$, thus facilitating the surface interaction. Our PCR results showed the long megastaple synthesis was very successful (Figure 12).

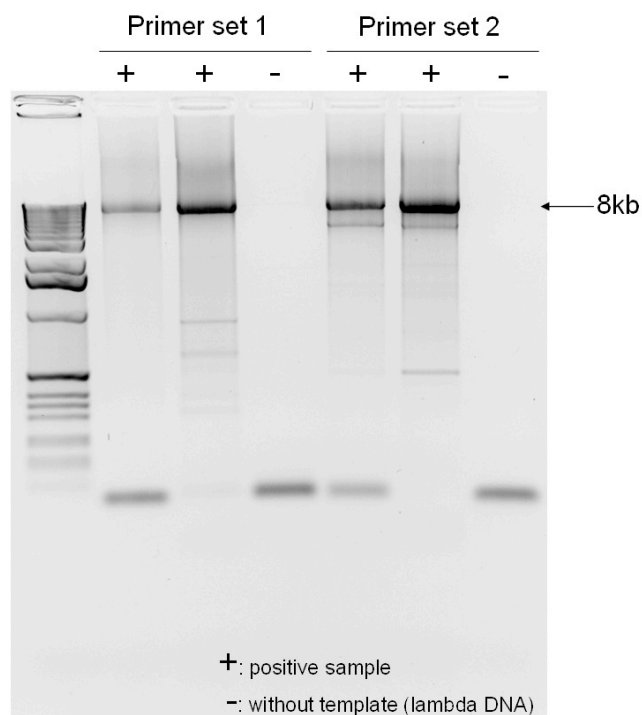


Figure 12. Agarose gel electrophoresis analysis of the PCR products. The desired length of the megastaple is about 8k base pairs, as indicated in the gel.

Milestone 2b: DNA-Mediated Surface Interaction

Overview

The target of Milestone 2b is to experimentally validate the ability of DNA hybridization to mediate the association of two DNA-conjugated surfaces. This is the key step of the entire project. Using molecular recognition to direct the assembly of mesoscale objects is a new fundamental concept in basic science and hasn't been demonstrated yet. Our recent efforts to validate this concept include two different approaches: (1) Using megastaples to direct the association of the mesoscale objects; (2) Using extremely long repetitive single-stranded DNA to direct mesoscale surface association.

(1) Megastaple-Directed Mesoscale Surface Association

Experimental design

We developed a fluorescence-transfer experiment to characterize the efficiency of megastaple-mediated surface interactions. In this experiment, fluorescent probe labeled megastaple is first hybridized to the surface-attached single stranded DNA. Then another surface with the complementary DNA single strands is brought into contact with the original surface. If the hybridization takes place, after separate the two surfaces, we should be able to see the fluorescence signals on the second surface (Figure 13).

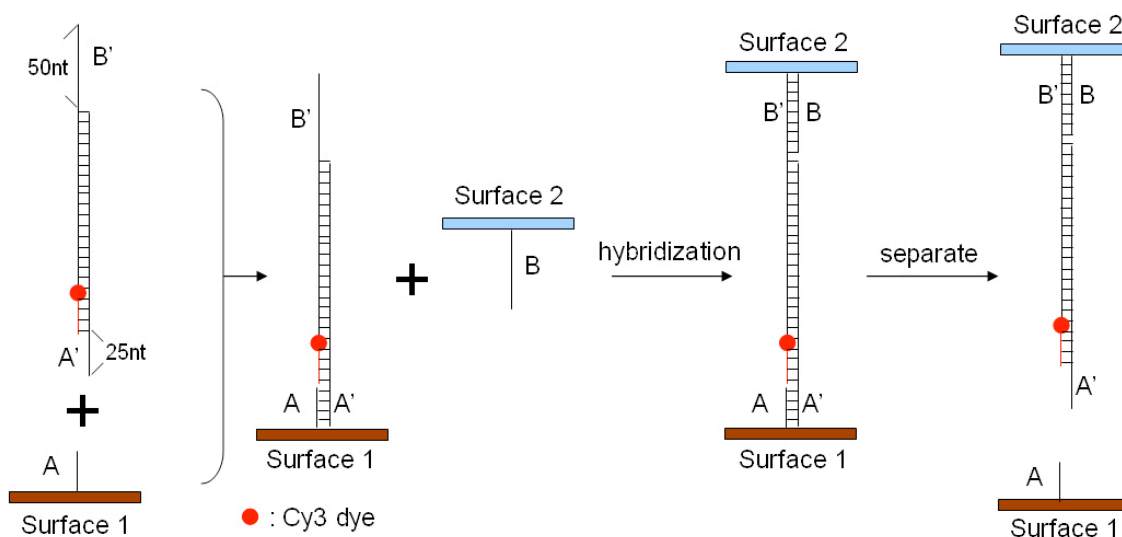


Figure 13. Scheme for a fluorescence-transfer experiment to characterize the efficiency of megastaple-mediated surface interactions. Fluorescent megastaple is first hybridized to oligonucleotides immobilized on Surface 1. Surface 2 is then brought into contact with Surface 1. After the two surfaces are separated, fluorescence should be observed on Surface 2 only if the megastaples were able to hybridize both surfaces simultaneously.

Results

From the experimental results, we can see that after surface separation, there is some fluorescence signal showed up on the second surface (Surface 2). The surface 2 is PDMS with 100μm protrudent square patterns. In the image, only the patterned area, which could effectively contact the Surface 1,

has signal, suggesting that the fluorescence transfer is due to a hybridization event involving the two surfaces in close contact.

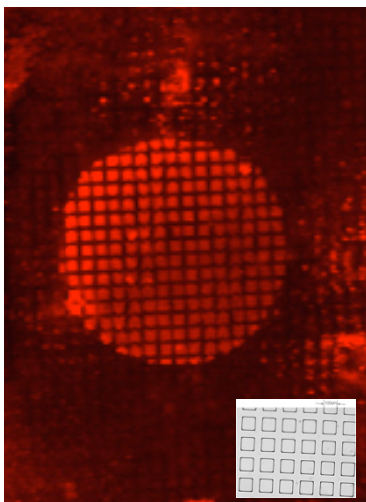


Figure 14. Fluorescence image of Surface 2 after DNA hybridization and surface separation. The fact that fluorescence signal is present on Surface 2 indicates that megastaples were able to hybridize both surfaces simultaneously. Additionally, the pattern of fluorescence corresponds to the raised areas patterned on to Surface 1 (microscope image, inset), suggesting that the fluorescence transfer is due to a hybridization event involving the two surfaces in close contact.

However, there are two major problems existing in the experiment. First, the reproducibility of this experiment is not very high (~30% so far), and sometimes we also got very strong background signals. A possible reason is that, we couldn't wash off all the free DNA strands after DNA attachment and hybridization, probably due to the hydrophobicity of the PDMS surface. Secondly, after the hybridization takes place between the two surfaces, we couldn't observe very strong interaction between the surfaces, which indicates the hybridization yield is still very low. In order to improve the reproducibility and also hybridization yield, we also tried a number of different approaches.

Approach 1: DNA-mediated interaction between gold surfaces

We tried to develop DNA-mediated gold surface interactions. Gold surface has some distinct properties other than glass and PDMS. Since flat gold surface can be easily made by metal evaporation and the gold-thiol interaction is very reliable and easy to carry out, it's quite feasible to introduce single stranded DNA onto the gold surface. Besides, free DNA single strands can be easily cleaned off from the gold surface, thus effectively lowering the background signals. Our experimental results showed that the fluorescent probe DNA can effectively hybridize to DNA that is attached onto the gold surface, while the negative control sample gave very weak fluorescent signal, indicating a much lower background (Figure 15a), as we expected.

We also performed the gold surface interaction experiment, as shown in Figure 15b. The thiolated ssDNA was first immobilized onto the gold surface. The surface was then passivated with mercaptohexanol. Subsequently, another complementary thiolated ssDNA was added and hybridized to

the surface bounded ssDNA. After a thorough washing step, another bare gold surface was brought into contact with the DNA modified gold surface and the two surfaces were incubated for overnight. After incubation, we observed some weak interaction between the two gold surfaces. And the negative control sample, which doesn't contain the thiol group, didn't show any interaction between the surfaces. This result was quite promising. However, the interaction was still quite weak. We hypothesized that the rigidity of the gold surface would inhibit the good conformal contact between the two surfaces, thus there was only a small portion of the surface bounded DNA can effectively participate the hybridization and the surface reactions, resulting in a much weaker surface interaction. Therefore, a softer and squeezable surface is expected to be a better choice.

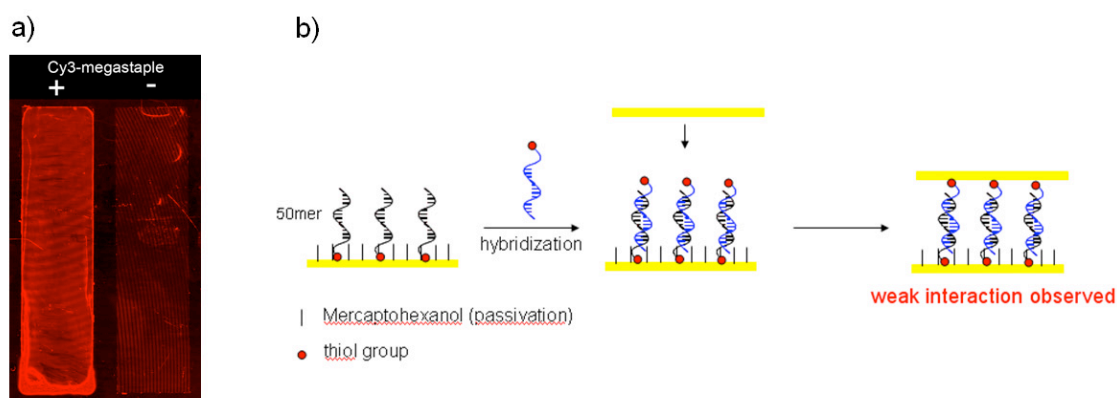


Figure 15. a) Fluorescence image of the gold surface after hybridization with the fluorescent megastaples. Left, the surface bounded ssDNA is complementary with the fluorescent megastaples; Right, the surface bounded ssDNA is not complementary with the fluorescent megastaples. b) The scheme of testing the gold surface interaction mediated by DNA hybridization.

Approach 2: DNA-mediated interaction between dendrimer coated surfaces

Dendrimers are repeatedly branched molecules, which could contain lots of hydrophilic functional groups. Using dendrimer coated surface as substrate to perform DNA-mediated surface interaction would have several potential advantages: 1) the densely packed functional groups could react with DNA molecules, thus increasing the surface DNA coverage and surface hydrophilicity. 2) Dendrimer molecules are about several nanometers in size. If the surfaces are modified with these bulky molecules, the surfaces would become softer and may better contact with each other, which could, therefore, facilitate DNA hybridization.

The protocol of immobilizing dendrimer molecules onto the surface is illustrated in Figure 16a. After immobilization of dendrimer molecules, single stranded amine DNA was added onto the surface, followed by the addition of the complementary fluorescent probe DNA. The hybridization assay results on both glass substrate and PDMS substrate are shown in Figure 16b. From the results, there are a number of things we learned:

- (1) ssDNA can be covalently linked onto the surfaces and further hybridize with complementary fluorescent DNA.

- (2) Dendrimer modification didn't improve the DNA density quite much compared with the non-dendrimer surface.
- (3) The glass surface, after modified with dendrimer and DNA, became fairly hydrophilic. However, the PDMS surface, after modified with dendrimer and DNA, was still not hydrophilic. This is a potential problem for the surface interaction.
- (4) The PDMS surface became a little blurry after all steps of modifications, probably due to the solvent-induced swelling and acid etching. Therefore, this protocol might not be a good way for the PDMS surface modification.

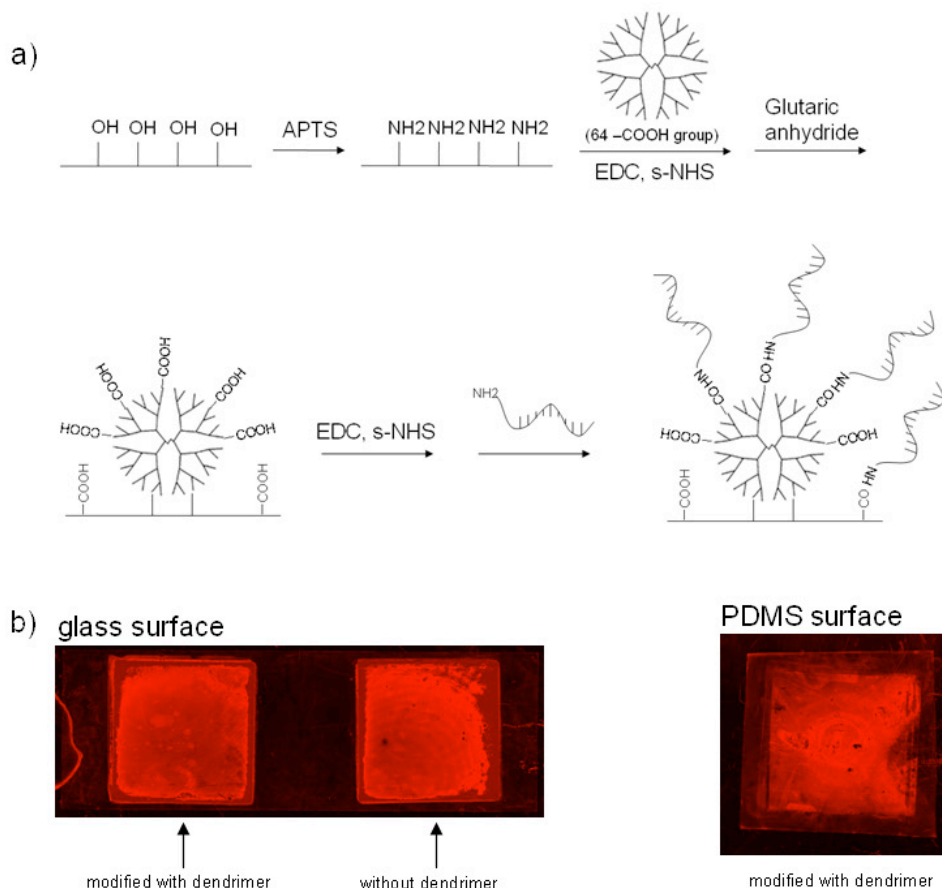


Figure 16. a) The procedure of immobilization of dendrimer molecules onto the surfaces. b) Fluorescence assay of the DNA hybridization on the dendrimer coated glass surface (left) and PDMS surface (right).

Approach 3: DNA-mediated interaction between polymer-coated surfaces

We also tried to immobilize DNA single strands onto the polymer coated glass slide. The polymer we chose has hydrophilic backbones. It also contains NHS ester that could react with amine DNA. The thickness of the polymer layer is about 10nm, which provides a slightly soft, squeezable surface. We used this polymer coated surface as substrate (Surface 1) and performed the fluorescence transfer experiment again.

In order to improve the reliability of the fluorescence-transfer experiment, we have redesigned the experiment to use megastaples with two fluorophores directly attached to them. Compared with our

previous version of fluorescent labeled megastaple, the new one has several additional advantages: 1) The fluorophore is covalently attached to the megastaple, meaning we do not have to worry about an extra intermolecular interaction; 2) One of the handles is no longer occluded for half its length. 3) Since there are fluorophores on both sides, there should be no difference in surface quenching on the top and bottom surfaces.

The experiment design is shown in Figure 17b. From the results, we observed fairly strong fluorescence signal on the positive PDMS surfaces after the transfer experiment. Meanwhile, the negative PDMS samples showed much lower fluorescence signal. The polymer coated glass slide also showed reasonable pattern after the transfer. The fluorescence signal in the contact area became much weaker. Moreover, we also observed some interaction between the PDMS and glass surfaces. All these phenomena suggested the DNA hybridization could mediate mesoscale surface interaction.

However, there are still a number of disadvantages of the polymer coated surface. Currently, the polymer coated surface is only available on the glass slides. It would be desired to prepare such a polymer coating on some other substrates. In addition, for the negative samples, we also observed some interaction between the two surfaces. That's probably because the polymer layer is relatively soft and squeezable. It could change surface morphology upon pressure during the DNA hybridization. This morphology change could also introduce some non-specific interaction between the surfaces. Therefore, the difference between the positive sample and the negative sample is not quite clear. We still need to further enhance the DNA hybridization induced specific surface interaction.

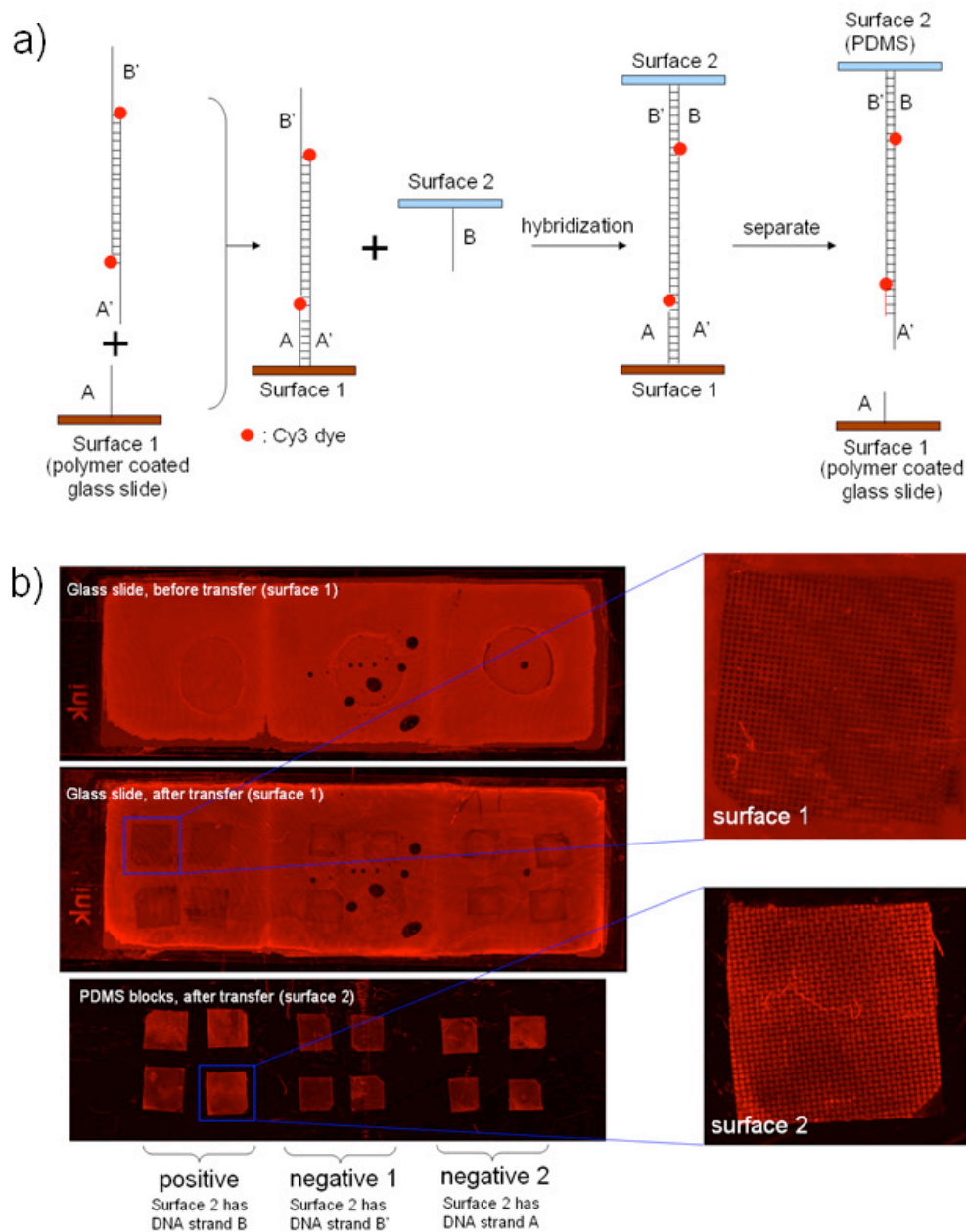


Figure 17. a) Scheme of a new version of fluorescence-transfer experiment. Note that in this version, a symmetric fluorescence labeled megastaple was employed. b) Fluorescence transfer experiment results.

Research In Progress Towards Milestone 2b (and the other Phase II milestones)

(1) Extremely long repetitive ssDNA-mediated surface association

Although our initial efforts on the megastaple-mediated surface interaction showed promising results, it still remains to be confirmed that DNA hybridization can induce strong mesoscale surface

interaction. In order to achieve more convincing results, we developed a new approach. Instead of using 50 base pairs of DNA hybridization to induce the surface interaction, we are now using single-stranded DNAs thousands of base pairs in length with highly repetitive sequences. If we can modify the two surfaces with complementary single stranded DNA with length of several thousand bases, the potential interaction between the two surfaces could be even higher than the theoretical Newton-scale interactions of the original design. As a result, realizing even a small fraction of the theoretically possible interactions in this new design may enable our basic vision of programmable matter to be realized.

Experimental design

We proposed to use rolling circle amplification (RCA) to prepare super long repetitive DNA single strand. The mechanism of RCA reaction is shown in Figure 18. It utilizes a small circular single stranded DNA as a template. At the presence of primer, polymerase, and dNTP, the primer can elongate along the circular template for multiple cycles, generating a super long (several thousand bases or even longer) repetitive single stranded DNA product. Another advantage of the repetitive sequences is that the two complementary DNA single strands can hybridize at any position. Consequently, using long repetitive ssDNA to mediate surface interaction could potentially tolerate much larger surface defects.

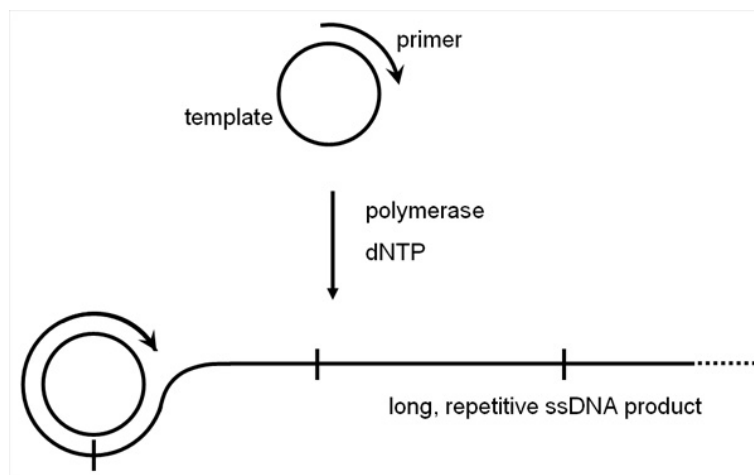


Figure 18. Mechanism of the rolling circle amplification reaction.

We proposed two approaches to carry out the experiments:

1. Approach A:
 - (1) Using RCA to generate two long repetitive single stranded DNA. The two primers both have a 5' amino group. The two circular templates are complementary to each other.
 - (2) Immobilize the obtained single-stranded DNA onto two surfaces
 - (3) Test and quantify the surface interactions.

2. Approach B:

- (1) Immobilize the two aminated DNA primers onto two different surfaces
- (2) RCA on surface to generate surface bounded long repetitive single-stranded DNA.
- (3) Test and quantify the surface interactions.

Initial Results

1. ligation of the circular template:

In order to perform RCA, we need a circular DNA as template. Therefore, the first task is to synthesize circular ssDNA via ligation. The ligation result is shown below:

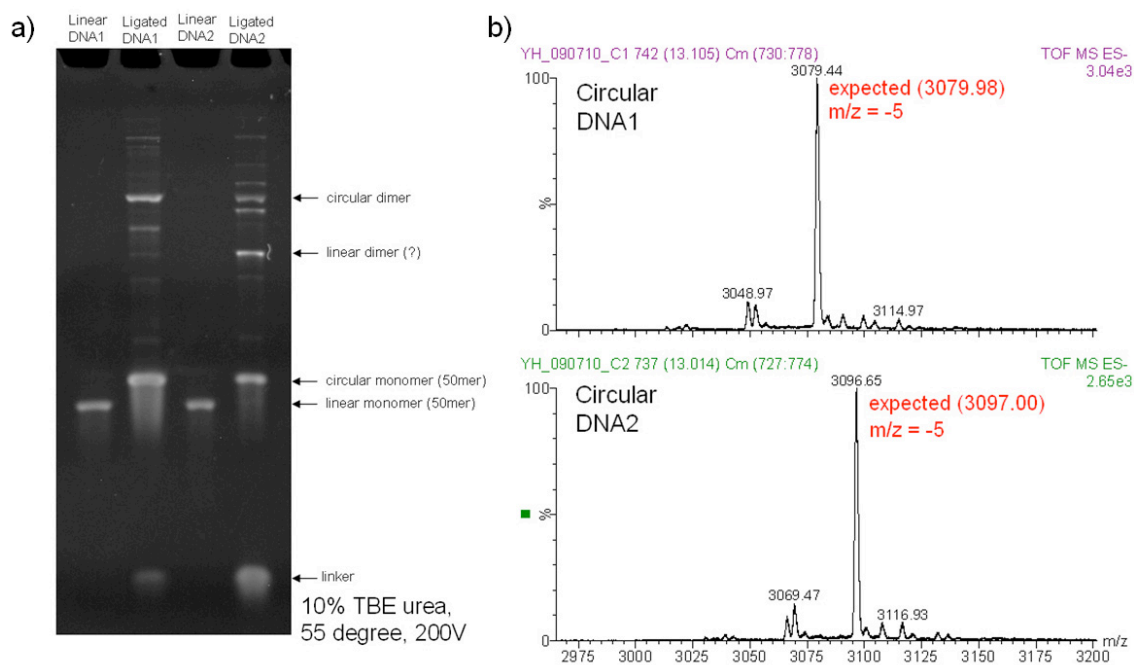


Figure 19. a) TBE-Urea polyacrylamide gel electrophoresis (PAGE) analysis of the ligated circular DNA templates. b) LC-MS characterization of the purified circular monomer DNA templates.

The ligation yield was good. It's quite evident that the major products we obtained were circular DNA. The circular monomer products were then further purified and characterized with LC-MS and the expected molecular weights were observed (Figure 19b).

2. RCA reaction:

The ligation products were used for the RCA at different DNA concentrations. The products were characterized with agarose gel electrophoresis. From the gel, super long DNA single strand products were observed, which indicated the RCA reaction in solution was very successful.

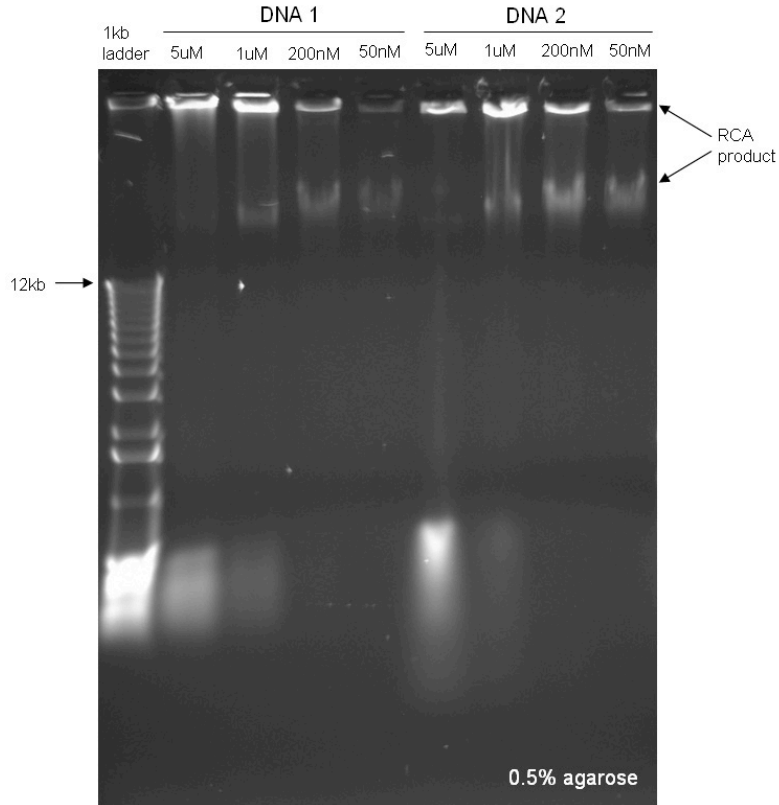


Figure 20. 0.5% agarose gel electrophoresis analysis of the RCA products.

3. RCA reactions on surfaces:

From the solution RCA reaction results, it seems the products were much longer than 10kb. Therefore, if we use such long ssDNA to do surface modification, the surface coupling efficiency would be very low (active amino group is embedded). Besides, it would be difficult to get sufficient amount of long ssDNA products to do the surface modification. So, we decided to start with **Approach B**: to directly generate long ssDNA on surface. After surface RCA reaction, fluorescent probe DNA was added onto the surface. The probe DNA could only hybridize with the RCA product, but not the primer. The fluorescent image clearly showed that RCA reaction on the surface was successful. In addition, the negative sample gave very weak fluorescent signals, indicating a low background.

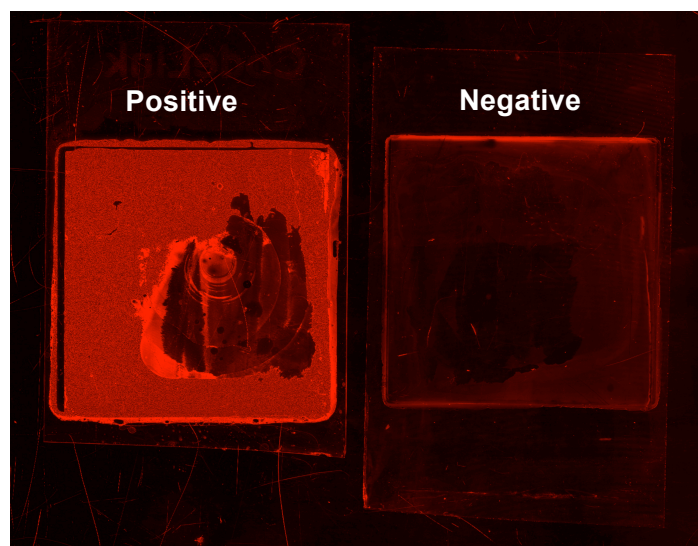


Figure 22. Fluorescent image of the surface RCA product incubated with fluorescent probe DNA.

Currently, we are further studying the RCA reactions on PDMS surface and also testing the surface interaction mediated with the RCA products.

Mid- to long-term challenges:

Currently, we are focusing on the DNA-mediated mesoscale surface interaction. This is not a trivial problem, from both scientific and technical point of view. We envision there are a number of critical issues we are facing to: how to achieve flat, soft, and hydrophilic DNA encoded surface; how to minimize non-specific surface interaction; how to get good conformal contact between two surfaces; and how to optimize DNA hybridization between the surfaces. We are on the way to solving these problems.

One of our mid-term challenges is that even if surfaces can interact through molecular recognition, it is quite another matter for them to adhere through transient contact while tumbling in solution. We might overcome this challenge by having a preliminary, weak nonspecific interaction between smartblock surfaces. This way, tumbling smartblocks would interact for a longer time, allowing the strong, specific interaction to occur, but allowing them to break up if mismatched.

Furthermore, there are a number of kinetic issues which will need to be dealt with. Our scheme is on its face based on a thermodynamic argument: the correct arrangement of smartblocks is the lowest-energy one, because it maximizes the amount of surface interactions. However, there are kinetic issues which may inhibit finding the thermodynamic minimum, such as off-center interactions and improper assembly order.

The problem with off-center interactions is that, while the correct orientation maximizes the surface contact and is thus a thermodynamic minimum, it is more likely for tumbling smartblocks to

meet each other off-center. The best solution to this would be to lower the kinetic barrier for interacting smartblocks to “slide” against each other, allowing the thermodynamic minimum to be reached more readily. (Figure 23)

Another kinetic issue is that if all smartblock surfaces are available to hybridize at once, the order of assembly will be uncontrolled, which could lead to problems like unoccupied lattice points (voids), and multiple nucleation sites causing regions of the object to partially coalesce separately. Preventing voids can be helped by selecting the best honeycomb lattice (e.g. truncated octahedra instead of cubes), but direct control of the assembly order would be a powerful solution to this problem. We have proposed a scheme for ordered self-assembly making use of DNA threshold gates which have been reported in the literature. (Figure 24)

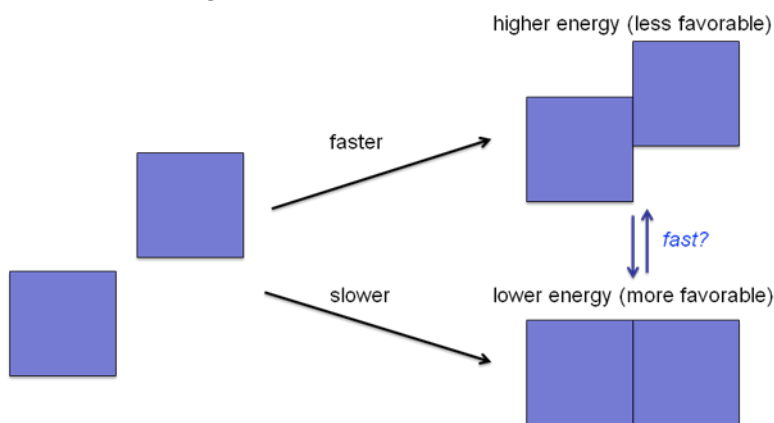


Figure 23. Schematic illustrating the problem of off-center interactions. The formation of the undesired off-center product is less thermodynamically favorable but more kinetically favored, indicating that smartblocks could get “stuck” in this arrangements. One way around this problem would be to minimize the kinetic barrier for directly converting off-center to on-center interactions, either through design or finding appropriate experimental conditions.

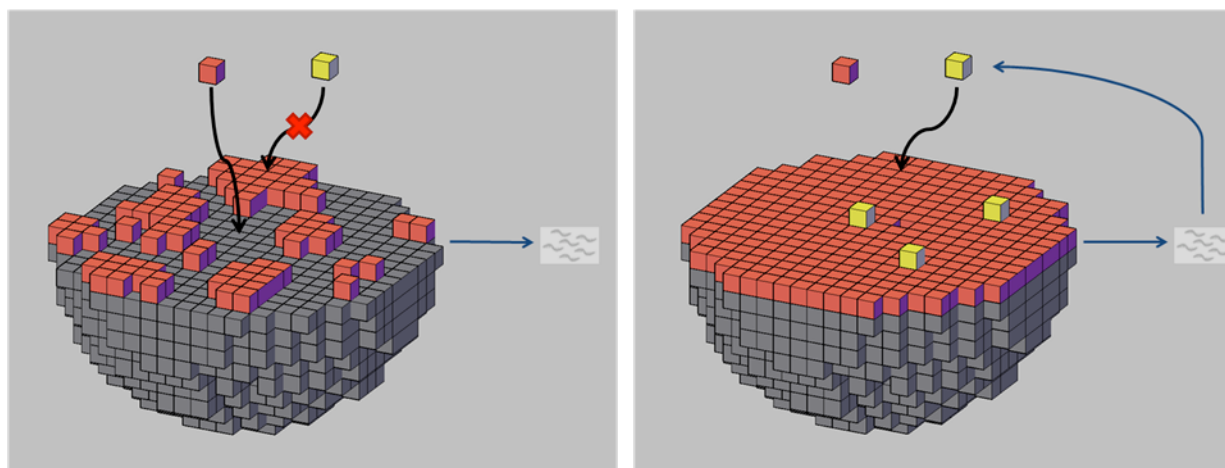


Figure 24. Scheme for ordered self assembly. *Left:* Initially, only smartblocks in the “red” layer can assemble; “yellow” smartblocks in the next layer cannot assemble because their DNA handles are occluded by another oligonucleotide. The red smartblocks have handles which release a messenger oligonucleotide into solution upon assembly. *Right:* Once most of the red layer has assembled, the messenger oligonucleotide concentration becomes great enough that it triggers a threshold gate in solution that activates the yellow smartblocks by removing the occlusion on their handles.

Once these challenges have been overcome is complete, we may look into crosslinking chemistry or other secondary steps to supplement the DNA-mediated interactions in order to mechanically strengthen the object once it is assembled. (Milestones 3a-3b)

We envision the following as possible downstream applications for this process (Phase III and beyond):


- DNA aptamers that bind strongly to a small-molecule, protein, or nucleic-acid target can be readily evolved in the laboratory. The ability of aptamers to undergo hybridization changes upon target binding is well-established. This can be applied as programmable matter sensors that undergo desired structural changes in the presence of a target molecule (e.g. TNT, chemical or biological warfare agents, etc.)
- The messenger DNAs released upon smartblock-megastaple hybridization, used in our ordered self-assembly scheme above, could also be used to induce the assembly or disassembly of other programmable matter structures by mediating or disrupting smartblock-megastaple pairing. In addition to allowing ordered assembly of one structure, it could enable communication between multiple structures (e.g. bistability), signal amplification, or communication with biological systems.
- Our design for programmable matter may be amenable to directed evolution. Random libraries of megastaples induce the assembly of random three-dimensional structures. The structures are selected for a desired property (the ability to adopt a particular shape, mechanical strength under load, etc.). Structures that survive selection are disassembled and their megastaples are amplified, mutated, and reselected to evolve optimal programmable matter solutions to the task of interest.

In conclusion, we believe that the properties of DNA make it very suitable as a platform for directing the assembly of programmable matter. We have achieved significant accomplishments towards this goal by developing the computational infrastructure needed to design DNA-mediated programmable matter, as well as creating and characterizing the components of our programmable matter scheme, the DNA-linked surfaces that will be used in smartblocks, the megastaples, and the super long repetitive single stranded DNA. We are currently testing these components to develop the first DNA hybridization-mediated mesoscale surface interaction, arguably the key tipping point of our proposal.

Acknowledgements

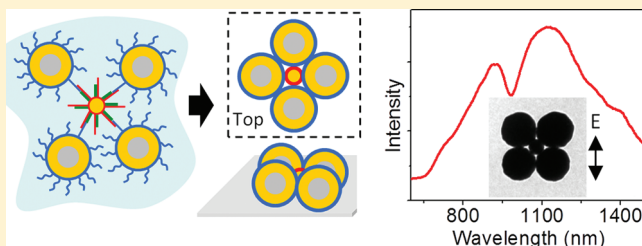
The Liu team consists of Dr. David Gorin, Dr. Yu He, Jia Niu, John Sadowski, and Prof. David Liu. This research was generously supported by DARPA.

DNA-Enabled Self-Assembly of Plasmonic Nanoclusters

Jonathan A. Fan,[†] Yu He,[‡] Kui Bao,[§] Chihhui Wu,^{||} Jiming Bao,[⊥] Nicholas B. Schade,[#] Vinodhan N. Manoharan,^{†,‡} Gennady Shvets,^{||} Peter Nordlander,[§] David R. Liu,[‡] and Federico Capasso^{*,†}[†]School of Engineering and Applied Sciences, Harvard University, 9 Oxford Street, Cambridge, Massachusetts 02138, United States[‡]Howard Hughes Medical Institute, Department of Chemistry and Chemical Biology, Harvard University, 12 Oxford Street, Cambridge, Massachusetts 02138, United States[§]Department of Physics, Rice University, 6100 Main Street, Houston, Texas 77005, United States^{||}Department of Physics, The University of Texas at Austin, One University Station C1500, Austin, Texas 78712, United States[⊥]Department of Electrical and Computer Engineering, University of Houston, 4800 Calhoun Road, Houston, Texas 77204, United States[#]Department of Physics, Harvard University, 17 Oxford Street, Cambridge, Massachusetts 02138, United States Supporting Information

ABSTRACT: DNA nanotechnology provides a versatile foundation for the chemical assembly of nanostructures. Plasmonic nanoparticle assemblies are of particular interest because they can be tailored to exhibit a broad range of electromagnetic phenomena. In this Letter, we report the assembly of DNA-functionalized nanoparticles into heteropentamer clusters, which consist of a smaller gold sphere surrounded by a ring of four larger spheres. Magnetic and Fano-like resonances are observed in individual clusters. The DNA plays a dual role: it selectively assembles the clusters in solution and functions as an insulating spacer between the conductive nanoparticles. These particle assemblies can be generalized to a new class of DNA-enabled plasmonic heterostructures that comprise various active and passive materials and other forms of DNA scaffolding.

KEYWORDS: Plasmonics, DNA, colloidal self-assembly, nanoshell, magnetic dipole, Fano resonance



Sub-wavelength-scale metallic particles are a basis for nanoscale light manipulation because they support localized surface plasmon resonances, which are oscillations of free electrons in metal that couple with electromagnetic waves.¹ By synthesizing particles into specific shapes and engineering their assembly, it is possible to construct nanoscale chemical sensors,² plasmonic rulers,³ optical nanocircuits,⁴ and metamaterials.^{5,6} DNA nanotechnology⁷ is a vehicle for the controllable assembly of nanoparticles⁸ because it enables the positioning of particles with nanoscale precision and the tailoring of their binding interactions. While simpler implementations of DNA particle assembly involve controlled nanoparticle aggregation,^{9,10} other efforts have focused on the construction of well-defined clusters and lattices. For example, micrometer-scale dielectric particles have been assembled into tetrahedral and octahedral clusters,¹¹ and in other schemes, trimer clusters,^{12,13} tetrahedral clusters,¹⁴ chiral helical assemblies,¹⁵ and two- and three-dimensional lattices^{16,17} of plasmonic nanoparticles have been constructed. It is tantalizing to envision these nanostructures as useful optical structures; however, these plasmonic assemblies have yielded little optical data in the literature because they typically utilize very small metallic particles (diameter <20 nm). With such small particles, optical measurements on individual nanostructures become

extremely difficult due to their small scattering cross sections. Larger optical signals can be obtained from ensemble measurements, but these suffer from sample heterogeneities that can weaken or completely eliminate the observation of certain optical resonances.¹⁸ Another issue with small particles is that, unlike large particles, they do not support many plasmonic modes; higher order resonances require retardation for their excitation, and Fano-like resonances, which will be discussed later, require strong linewidth broadening from radiative damping and retardation that exist only in large particle systems.

In this study, we use DNA to construct heteropentamer clusters consisting of a solid gold nanosphere surrounded by four larger nanoshells.¹⁹ The DNA route to particle assembly has distinct advantages over previous random capillary assembly methods:⁶ it introduces more specific and programmable interactions between metallic particles of different sizes and types and provides a potential route to more sophisticated three-dimensional particle assembly. The construction of the heteropentamer was partially motivated by prior calculations demonstrating

Received: August 3, 2011

Revised: October 10, 2011

Published: October 18, 2011

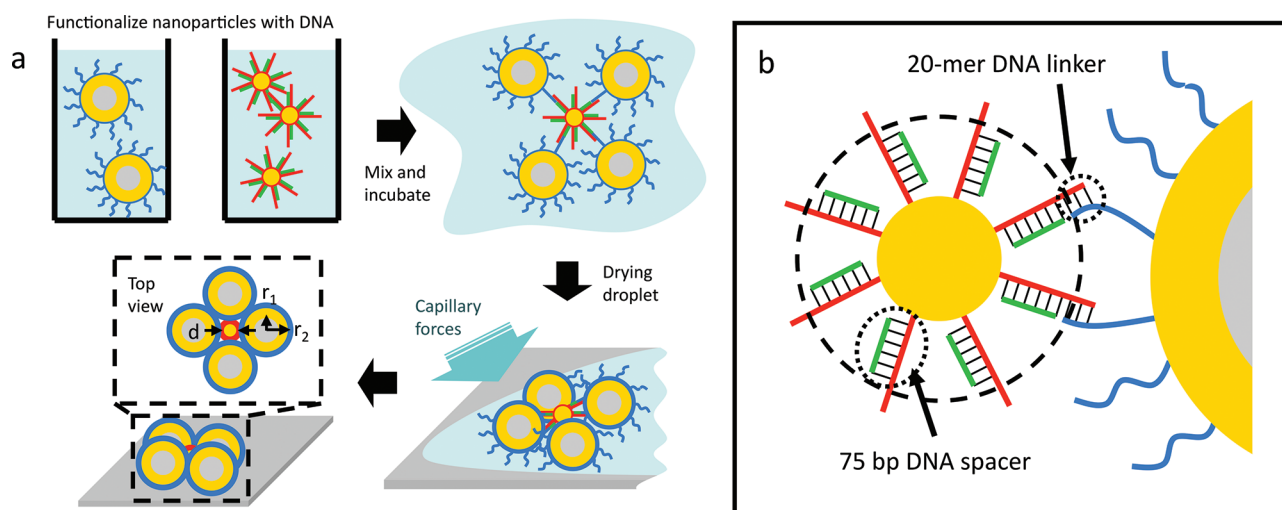


Figure 1. DNA-mediated assembly of plasmonic heteropentamers. (a) To assemble the clusters, gold nanospheres and nanoshells are functionalized separately with thiolated DNA strands, which form self-assembled monolayers on the particle surfaces. They are then mixed and incubated together at room temperature, where they assemble into “loosely” bound pentamers. Finally, the clusters are dried on a hydrophilic substrate, where capillary forces compress the pentamers into a close-packed two-dimensional configuration. (b) The nanospheres are functionalized with partially dsDNA molecules consisting of three regions: a gold attachment region comprising a thiol group and 5-mer polyT sequence, a 75bp ds “spacer” region, and a 20-mer “linker” region. Prior to nanosphere attachment, the thiolated 100-mer DNA (red) is mixed with complementary 75-mer strands (green) to form rigid dsDNA segments that effectively increase the nanosphere size in solution (dotted circle). The nanoshells are functionalized with ssDNA (blue) comprising a 50-mer polyT spacer sequence, followed by a 20-mer linker that complements the nanosphere linker.

Fano-like resonances for this cluster geometry;²⁰ sufficiently large nanoparticles are used here so that the Fano minima are clearly observable. The ratio of the nanoshell diameter to nanosphere diameter is set to approximately 2.4 to ensure a close packed geometry and strong coupling between all neighboring particles.

The self-assembly process is outlined in Figure 1a. First, the nanospheres and nanoshells are functionalized separately with different thiolated DNA molecules,²¹ which form self-assembled monolayers on the particle surfaces. The outermost 20-mers of DNA on the nanospheres and nanoshells are complementary, thus facilitating specific nanosphere–nanoshell binding while minimizing interactions between particles of the same type (Figure 1b). The particles are then cleaned and incubated together at high salt concentration and room temperature, where loosely packed pentamers are formed in three dimensions in aqueous suspension. The ratio of the number of nanoshells to nanospheres is set to 12:1 to enhance pentamer yield while limiting the assembly of large nanoshell–nanosphere aggregates, which were observed for particle mixtures with smaller ratios. Finally, the clusters are air-dried on a hydrophilic substrate at room temperature. During the drying process, capillary forces compress these loosely packed three-dimensional structures into two-dimensional pentamers. Both single-stranded DNA (ssDNA) and double-stranded DNA (dsDNA) collapse and pack to yield dense 2 nm thick dielectric spacers between all neighboring nanoparticles, ensuring their strong and controlled optical coupling. As a control experiment, nanoparticles were functionalized with non-complementary DNA sequences and mixed together, and no pentamers were observed. It is difficult to quantify the overall yield of these pentamer clusters (further discussed in the Supporting Information); nevertheless, it is easy to find many pentamers on a TEM grid, which is sufficient for single nanostructure experimentation. We also found other DNA-enabled clusters, ranging from dimers and trimers to small aggregates. Heteropentamer yields may be further enhanced by

increasing the number ratio of nanoshells to nanospheres and employing separation methods, such as density gradient centrifugation, to distill pentamers from single nanoshells and other cluster types, and this will be the subject of future study.

The assembly of pentamers in solution involves the sequential attachment of nanoshells onto a nanosphere (Figure 2a). The first association between a single nanoshell and nanosphere is straightforward: Brownian motion brings the two particles into close proximity and their surface-attached DNA hybridizes. However, the association of additional nanoshells onto a nanosphere becomes more difficult kinetically for two principal reasons (Figure 2b). The first involves steric hindrance: already associated nanoshells will physically block other nanoshells from getting close to and associating with the nanosphere. The second is due to the lack of hybridizable DNA on the nanosphere surface. Single-stranded DNA is a polymer with $\sim 1\text{--}2$ nm persistence length in solutions containing high salt concentration (ref 22), such that multiple DNA strands from a single nanoshell can attach to multiple nanosphere DNA strands in a polyvalent interaction. In our system where the length of DNA is on the order of the nanosphere diameter, the DNA from two or three nanoshells can associate with most of the nanosphere strands, leaving very few free nanosphere strands for additional association events. In order to overcome these problems, we design the 75 base double-stranded spacer on the nanosphere. Since the persistence length of dsDNA is 50 nm, this rigid spacer effectively increases the size of the nanosphere in solution by 50 nm^{23} (Figure 1b), alleviating the steric hindrance problem. Also, the rigidity of the dsDNA and relatively short length of the ssDNA linker reduce the polyvalent association between the nanoshells and nanospheres.

Individual heteropentamers are identified using transmission electron microscopy (TEM), and scattering spectra from individual clusters are measured in the near-infrared frequency range using dark-field microscopy. (See Supporting Information for setup.) Here, the incident light is s-polarized (i.e., the electric

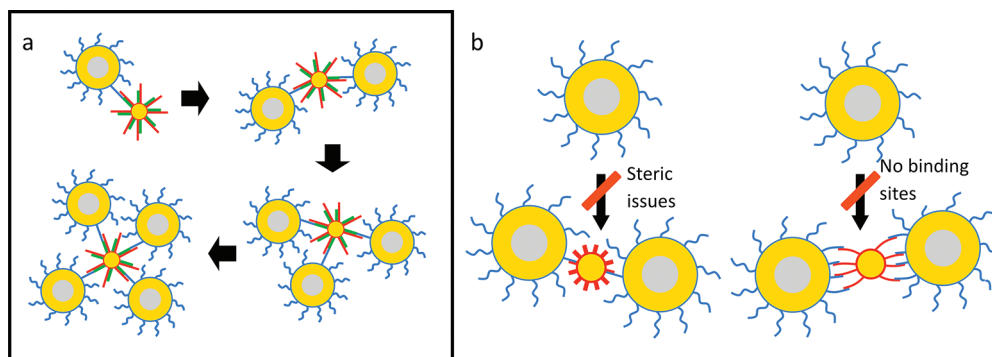


Figure 2. Detailed view of plasmonic cluster formation in solution. (a) The pentamer assembles in solution by the sequential attachment of nanoshells onto a nanosphere. Successful pentamer assembly requires each of these intermediate steps to be stable (i.e., the nanoshells remain attached) and kinetically accommodating to additional nanoshell association events. (b) There exist at least two issues that can impede the attachment of additional nanoshells to a cluster. One is that already associated nanoshells can sterically hinder other single nanoshells from getting close to and attaching to the nanosphere (left). This is especially a problem if the nanosphere DNA strands are too short. Another is that if the nanosphere DNA is too long and floppy, DNA from just two or three nanoshells can associate with most of the nanosphere DNA, reducing the total number of available linker DNA on the nanosphere and suppressing additional nanoshell association events (right). Both of these issues are addressed by utilizing the long dsDNA spacer on the nanosphere.

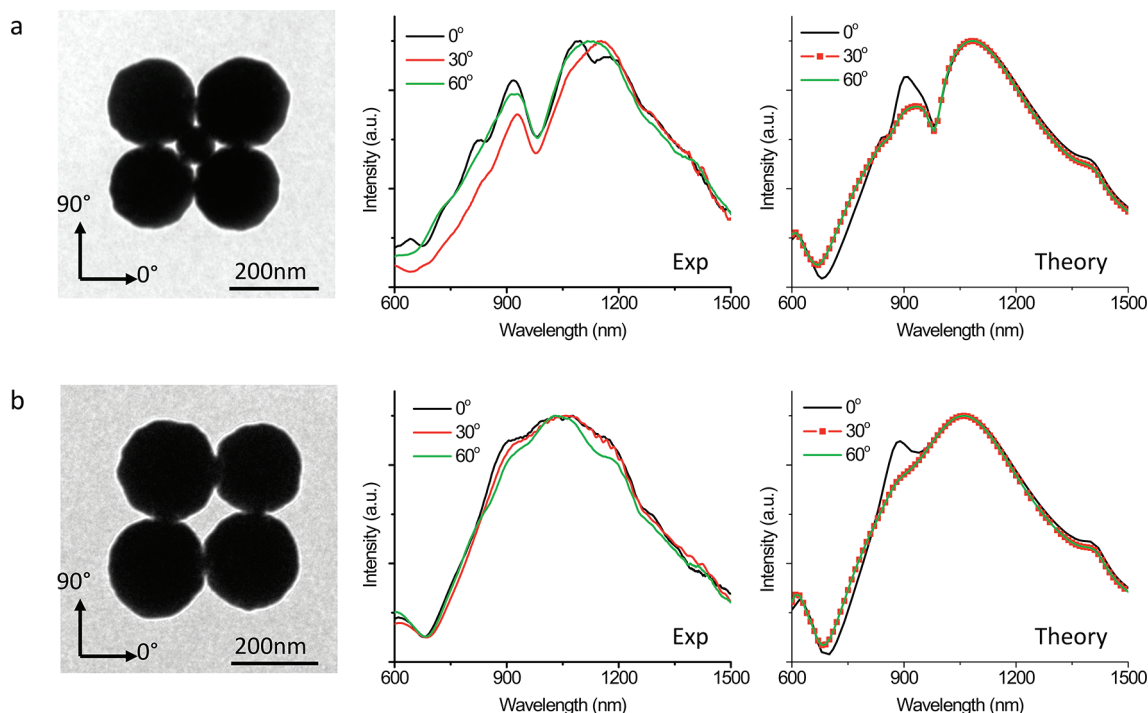


Figure 3. TEM images and scattering spectra of individual heteropentamer and quadramer clusters. (a) s-polarized spectra of a pentamer for different electric field polarization angles. Both the experimental and theoretical spectra are characterized by a broad electric dipole peak and a narrow Fano dip near 1000 nm. The in-plane isotropy of these spectra is consistent with the symmetry of these clusters. The simulated geometry is based on the TEM image and uses a nanosphere diameter $d = 74$ nm, nanoshell $[r_1, r_2] = [62.5, 92.5]$ nm, and interparticle gaps of 2 nm that are filled with dielectric. (b) TEM image and s-polarized spectra of a symmetric quadramer. These spectra exhibit a broad electric dipole peak but no clear Fano dip, indicating that the nanosphere is necessary for this cluster system to exhibit a strong Fano-like resonance. The experimental spectra generally match those simulated using the same nanoshell geometry and gap dielectric as in (a).

field is in the plane of the cluster) and the polarization angle of the electric field relative to the nanostructure is controlled. Scattered light from an individual structure is selected with a confocal-type technique, by placing a pinhole at a reimaged focal plane and allowing light from only the structure of interest to enter the spectrometer. Spectra of a single pentamer for three different polarization angles are shown in Figure 3a and are

characterized by a broad electric dipole resonance spanning the entire range of the plot. There exists a narrow and asymmetric dip near 1000 nm, which is a Fano resonance. These resonances arise from interference between a superradiant “bright” mode and a subradiant “dark” mode and have been studied extensively in plasmonic systems.^{5,24} These experimental spectra match those calculated using the finite element simulation software

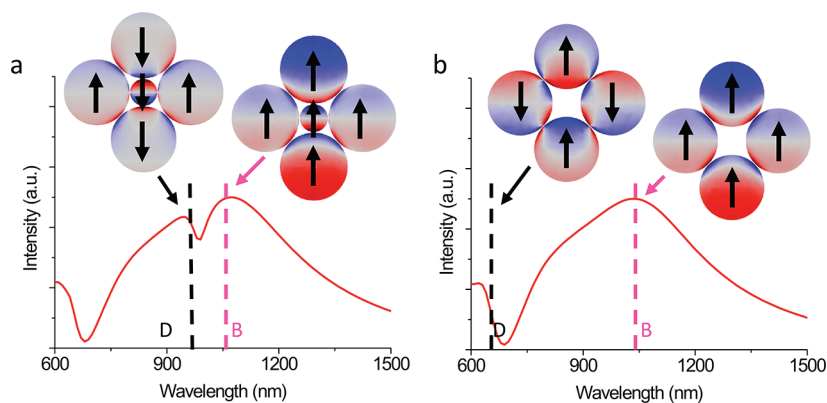


Figure 4. Theoretical analysis of the bright and dark modes involved with Fano-like resonances. (a) Extinction spectrum and surface charge plots of the heteropentamer excited at normal incidence with a 45° polarization angle. The charge density of the bright mode, which is peaked at 1050 nm (pink dashed line), shows the charge oscillations on each nanoparticle oriented in the same direction, yielding a large cluster dipole moment. The dark mode at 980 nm (black dashed line) shows the charge oscillations on each nanoparticle oriented in different directions, yielding a small cluster dipole moment and suppressed radiative losses. There is clear capacitive coupling between the nanosphere and the two nanoshells above and below the nanosphere, which redshifts the mode close to the bright mode peak. (b) Extinction spectrum and surface charge plots of the quadramer excited with the same conditions as in (a). The bright mode peak is near 1040 nm (pink dashed line) and the charge distribution shows a large cluster dipole moment. The dark mode peaked at 650 nm (black dashed line) shows the total cluster dipole moment is small. The absence of capacitive coupling between the nanoparticles prevents strong overlap in frequency between the dark and bright modes.

COMSOL (Figure 2a) and are nearly independent of incident polarization angle due to the D_{4h} group symmetry of the cluster, which supports isotropic in-plane resonances in the quasistatic limit.

To further probe the interaction of the nanosphere with the nanoshells in the pentamer, we identified and optically characterized symmetric nanoshell quadramers. These nanostructures assembled by entirely different means from the pentamer: here, four single nanoshells trapped in a drying droplet clustered together by capillary forces, in similar fashion to clusters assembled previously.⁶ The strong electrostatic repulsion between the nanoshells, provided by the negatively charged DNA, helps them arrange in a non-close packed configuration; it is noted that in previous experiments utilizing uncharged PEG-functionalized nanoshells, symmetric quadramers were not found.⁶ The spectra from an individual quadramer display a broad electric dipole resonance but no strong Fano dips, indicating that the nanosphere in the pentamer is required for strong Fano-like resonances to be observed (Figure 3b). As with the pentamer, this cluster possesses isotropic in-plane resonances due to its group symmetry.

The Fano-like resonances in these clusters are further analyzed by examining the surface charge distributions of their bright and dark modes (Figure 4). In both the quadramer and pentamer, the bright modes are characterized by nanoparticle polarizations oriented in the same direction. As such, the cluster dipole moments are large and the mode strongly redshifts due to strong capacitive coupling between neighboring nanoparticles. Physically, this coupling arises from the attractive quasi-static interaction between surface charges on these nearly touching particles.²⁵ The dark modes of each cluster, however, have very different spectral positions. The pentamer dark mode charge distribution shows that the small nanosphere capacitively couples with two of the nanoshells, which strongly redshifts the mode. The total dipole moment of this cluster is small but non-negligible, which limits the magnitude of the Fano dip. The quadramer dark mode, which has been studied elsewhere,²⁶ exhibits little capacitive coupling between adjacent nanoshells. As a result, the mode is

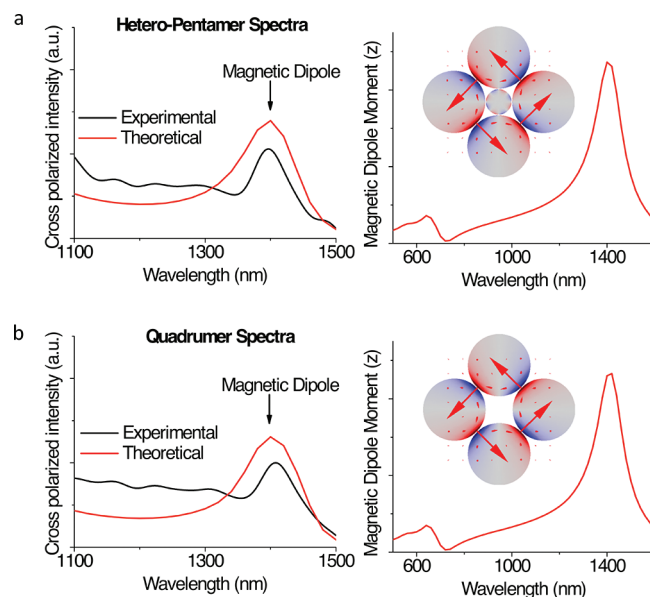


Figure 5. Magnetic dipole resonances in nanoparticle clusters. (a) Experimental and theoretical cross-polarized spectra of the pentamer at 0° polarization angle (left) reveal a narrow peak near 1400 nm, which matches the peak position of the calculated out-of-plane magnetic dipole moment of the cluster (right). The inset is a quasistatic mode plot of the surface charges (color) and displacement current (arrows) of the magnetic dipole mode. (b) Experimental and theoretical cross-polarized spectra of the quadramer with the same electric field polarization angle (left) also reveal a narrow magnetic dipole peak near 1400 nm that matches the peak position of the calculated magnetic dipole moment (right) of the cluster. The inset is a quasi-static mode plot of the magnetic dipole mode and shows a circulating current around the ring of nanoshells similar to that in (a). These plots and calculated magnetic dipole moments show that the magnetic dipole mode in the pentamer and quadramer is due to near-field interactions between the nanoshells and that the mode in the pentamer is effectively decoupled from the nanosphere.

blueshifted beyond the bright mode and there is no clearly visible Fano minimum. As observed with other nanocluster structures previously studied,⁷ the key to engineering a strong Fano dip is to design bright and dark modes that exhibit similar levels of capacitive coupling between particles, thereby enforcing strong spectral overlap between the two modes.

We also analyze magnetic dipole modes in these clusters. These resonances are excited by the magnetic component of the incident electromagnetic field and were previously measured in nanoshell trimers.⁶ They are predicted to be supported here by the outer ring of nanoshells, which form a closed loop of metallic nanoinductors and dielectric nanocapacitors²⁷ in similar fashion to the trimer. These modes are not clearly visible in the scattering spectra in Figure 5 because they weakly scatter compared to the electric dipole; a cross-polarizer oriented 90° relative to the incident light polarization can be placed after the collection objective to filter out elastically scattered electric dipole radiation.⁶ The cross-polarized spectra of the quadramer and pentamer are shown in Figure 5 and they both exhibit clear, narrow peaks near 1400 nm. The positions of these peaks match those of the calculated magnetic dipole moments, confirming that they are magnetic resonances. There is less background in these spectra compared to those of the trimer previously studied because unlike the trimer, these clusters have inversion symmetry and, based on the criteria outlined in ref 28, do not support extensive optical activity. The simulated electric field profile and displacement current of this mode in both cluster types show a circulating current around the quadramer ring, which is a hallmark of a classical magnetic dipole. The matching magnetic dipole moments from both clusters indicate that the presence of the nanosphere in the pentamer does not affect the magnetic resonance from the nanoshell ring. This can be further understood by group theory, in which the irreducible representation of the pentamer can be expressed as $\Gamma_{\text{Pent}} = \Gamma_{\text{Nanosphere}} + \Gamma_{\text{Quad}}$. The magnetic mode in the quadramer has an irreducible representation of A_{2g} while the nanosphere has a irreducible representation of E_{1u} ; as modes with different representations do not couple with each other, the nanosphere does not affect the magnetic mode.

The DNA-enabled assembly of nanoparticles can be generalized to a broad range of two- and three-dimensional heteroclusters. These are not limited to passive plasmonic particles and can include other types of dielectric, nonlinear, active, and organic materials to create new functional nanostructures such as active antennas,²⁹ surface plasmon lasers,³⁰ clusters with tailorable hot spots,³¹ and metamaterial fluids.³² Other forms of DNA nanotechnology, such as DNA origami,³³ have great potential as rigid scaffolds with high spatial resolution for particle assembly. In this study, the pentamers were assembled in two steps, first by DNA to “loosely” assemble the clusters in suspension and then by capillary forces to “compact” the clusters in two dimensions; loosely assembled clusters can be compacted or manipulated in three dimensions in suspension via depletion³⁴ or optical forces³⁵ or by tailoring new chemical interactions between particles,³⁶ and new regimes of capillary assembly can be employed using patterned substrates,³⁷ surfactants, or other additives to further control cluster assembly on substrates. The merging of biomaterials like DNA with plasmonic nanostructures is suggestive of new forms of plasmon-enhanced biomolecular detection schemes, dynamically reconfigurable nanostructure geometries, and even direct integration and assembly of nanoclusters within biological systems.

■ ASSOCIATED CONTENT

S Supporting Information. Materials and methods details. This material is available free of charge via the Internet at <http://pubs.acs.org>.

■ AUTHOR INFORMATION

Corresponding Author

*E-mail: capasso@seas.harvard.edu.

■ ACKNOWLEDGMENT

Electron microscopy was performed at the Center for Nanoscale Science at Harvard University, a member of the National Nanotechnology Infrastructure Network. J.A.F. and F.C. acknowledge the NSF Nanoscale Science and Engineering Center (NSEC). J.A.F. acknowledges M. Holmes-Cerfon for helpful discussions, H. Park and C. Yu for chemical storage, and D. Bell for EM support. Y.H. and D.R.L. acknowledge support from DARPA W911NF-08-1-0151, NIH/NIGMS (R01GM065865), and HHMI. P.N. and K.B. acknowledge support from the Robert A. Welch foundation (C-1222), the US Department of Defense NSEFF program (N00244-09-1-0067), and the Office of Naval Research (N00244-09-1-0989). C.W. and G.S. acknowledge the support from the Air Force Office of Scientific Research (FA8650-090-D-5037) and from the Office of Naval Research (N00014-10-1-0929). J.M. B. acknowledges support from the Robert A. Welch Foundation (E-1728). N.B.S. is supported in part by the Department of Energy Office of Science Graduate Fellowship Program (DOE SCGF), administered by ORISE-ORAU under contract no. DE-AC05-06OR23100. V.N.M. and F.C. acknowledge support from the NSF NIRT program (ECCS-0709323).

■ REFERENCES

- (1) Barnes, W. L.; Dereux, A.; Ebbesen, T. W. Surface plasmon subwavelength optics. *Nature* **2003**, *424*, 824–830.
- (2) Xu, H. X.; Bjerneld, E. J.; Kall, M.; Borjesson, L. Spectroscopy of single hemoglobin molecules by surface enhanced Raman scattering. *Phys. Rev. Lett.* **1999**, *83*, 4357–4360.
- (3) Sonnichsen, C.; Reinhard, B. M.; Liphardt, J.; Alivisatos, A. P. A molecular ruler based on plasmon coupling of single gold and silver nanoparticles. *Nat. Biotechnol.* **2005**, *23*, 741–745.
- (4) Engheta, N. Circuits with light at nanoscales: Optical nanocircuits inspired by metamaterials. *Science* **2007**, *317*, 1698–1702.
- (5) Luk'yanchuk, B.; et al. The Fano resonance in plasmonic nanostructures and metamaterials. *Nat. Mater.* **2010**, *9*, 707–715.
- (6) Fan, J. A.; et al. Self-Assembled Plasmonic Nanoparticle Clusters. *Science* **2010**, *328*, 1135–1138.
- (7) Seeman, N. C. DNA in a material world. *Nature* **2003**, *421*, 427–431.
- (8) Tan, S. J.; Campolongo, M. J.; Luo, D.; Cheng, W. L. Building plasmonic nanostructures with DNA. *Nat. Nanotechnol.* **2011**, *6*, 268–276.
- (9) Mirkin, C. A.; Letsinger, R. L.; Mucic, R. C.; Storhoff, J. J. A DNA-based method for rationally assembling nanoparticles into macroscopic materials. *Nature* **1996**, *382*, 607–609.
- (10) Rosi, N. L.; Mirkin, C. A. Nanostructures in bionanotechnology. *Chem. Rev.* **2005**, *105*, 1547–1562.
- (11) Soto, C. M.; Srinivasan, A.; Ratna, B. R. Controlled assembly of mesoscale structures using DNA as molecular bridges. *J. Am. Chem. Soc.* **2002**, *124*, 8508–8509.
- (12) Alivisatos, A. P.; et al. Organization of “nanocrystal molecules” using DNA. *Nature* **1996**, *382*, 609–611.

- (13) Hung, A. M.; et al. Large-area spatially ordered arrays of gold nanoparticles directed by lithographically confined DNA origami. *Nat. Nanotechnol.* **2010**, *5*, 121–126.
- (14) Mastroianni, A. J.; Claridge, S. A.; Alivisatos, A. P. Pyramidal and Chiral Groupings of Gold Nanocrystals Assembled Using DNA Scaffolds. *J. Am. Chem. Soc.* **2009**, *131*, 8455–8459.
- (15) Sharma, J.; et al. Control of Self-Assembly of DNA Tubules Through Integration of Gold Nanoparticles. *Science* **2009**, *323*, 112–116.
- (16) Zhang, J. P.; Liu, Y.; Ke, Y. G.; Yan, H. Periodic square-like gold nanoparticle arrays templated by self-assembled 2D DNA nanogrids on a surface. *Nano Lett.* **2006**, *6*, 248–251.
- (17) Nykypanchuk, D.; Maye, M. M.; van der Lelie, D.; Gang, O. DNA-guided crystallization of colloidal nanoparticles. *Nature* **2008**, *451*, 549–552.
- (18) Mock, J. J.; Barbic, M.; Smith, D. R.; Schultz, D. A.; Schultz, S. Shape effects in plasmon resonance of individual colloidal silver nanoparticles. *J. Chem. Phys.* **2002**, *116*, 6755–6759.
- (19) Oldenburg, S. J.; Averitt, R. D.; Westcott, S. L.; Halas, N. J. Nanoengineering of optical resonances. *Chem. Phys. Lett.* **1998**, *288*, 243–247.
- (20) Bao, K.; Mirin, N.; Nordlander, P. Fano resonances in planar silver nanosphere clusters. *Appl. Phys. A: Mater. Sci. Process.* **2010**, *100*, 333–339.
- (21) Hurst, S. J.; Lytton-Jean, A. K. R.; Mirkin, C. A. Maximizing DNA loading on a range of gold nanoparticle sizes. *Anal. Chem.* **2006**, *78*, 8313–8318.
- (22) Tinland, B.; Pluen, A.; Sturm, J.; Weill, G. Persistence Length of Single-Stranded DNA. *Macromolecules* **1997**, *30*, 5763–5765.
- (23) The persistence length of dsDNA is approximately 50 nm, and the total length is calculated from 150 total base pairs at 0.3 nm per base pair.
- (24) Hentschel, M.; et al. Transition from Isolated to Collective Modes in Plasmonic Oligomers. *Nano Lett.* **2010**, *10*, 2721–2726.
- (25) Nordlander, P.; Oubre, C.; Prodan, E.; Li, K.; Stockman, M. I. Plasmon hybridization in nanoparticle dimers. *Nano Lett.* **2004**, *4*, 899–903.
- (26) Fan, J. A.; et al. Fano-like Interference in Self-Assembled Plasmonic Quadramer Clusters. *Nano Lett.* **2010**, *10*, 4680–4685.
- (27) Alu, A.; Salandrino, A.; Engheta, N. Negative effective permeability and left-handed materials at optical frequencies. *Opt. Express* **2006**, *14*, 1557–1567.
- (28) Plum, E.; et al. Metamaterials: Optical Activity without Chirality. *Phys. Rev. Lett.* **2009**, *102*, 113902.
- (29) Knight, M. W.; Sobhani, H.; Nordlander, P.; Halas, N. J. Photodetection with Active Optical Antennas. *Science* **2011**, *332*, 702–704.
- (30) Noginov, M. A.; et al. Demonstration of a spaser-based nanolaser. *Nature* **2009**, *460*, 1110–U1168.
- (31) Li, K.; Stockman, M. I.; Bergman, D. J. Self-Similar Chain of Metal Nanospheres as an Efficient Nanolens. *Phys. Rev. Lett.* **2003**, *91*, 227402.
- (32) Urzhumov, Y. A.; et al. Plasmonic nanoclusters: a path towards negative-index metafluids. *Opt. Express* **2007**, *15*, 14129–14145.
- (33) Rothmund, P. W. K.; Folding, D. N. A. to create nanoscale shapes and patterns. *Nature* **2006**, *440*, 297–302.
- (34) Meng, G.; Arkus, N.; Brenner, M. P.; Manoharan, V. N. The Free-energy Landscape of Clusters of Attractive Hard Spheres. *Science* **2010**, *327*, 560–563.
- (35) Xu, H. X.; Kall, M. Surface-plasmon-enhanced optical forces in silver nanoaggregates. *Phys. Rev. Lett.* **2002**, *89*, 246802.
- (36) Valignat, M. P.; Theodoly, O.; Crocker, J. C.; Russel, W. B.; Chaikin, P. M. Reversible self-assembly and directed assembly of DNA-linked micrometer-sized colloids. *Proc. Natl. Acad. Sci. U.S.A.* **2005**, *102*, 4225–4229.
- (37) Yin, Y. D.; Lu, Y.; Gates, B.; Xia, Y. N. Template-assisted self-assembly: A practical route to complex aggregates of monodispersed colloids with well-defined sizes, shapes, and structures. *J. Am. Chem. Soc.* **2001**, *123*, 8718–8729.

A Sequential Strand-Displacement Strategy Enables Efficient Six-Step DNA-Templated Synthesis

Yu He and David R. Liu*

Howard Hughes Medical Institute, Department of Chemistry and Chemical Biology, Harvard University, 12 Oxford Street, Cambridge, Massachusetts 02138, United States.

S Supporting Information

ABSTRACT: We developed a sequential strand-displacement strategy for multistep DNA-templated synthesis (DTS) and used it to mediate an efficient six-step DTS that proceeded in 35% overall yield (83% average yield per step). The efficiency of this approach and the fact that the final product remains linked to a DNA sequence that fully encodes its reaction history suggests its utility for the translation of DNA sequences into high-complexity synthetic libraries suitable for in vitro selection.

DNA-templated synthesis (DTS), the use of DNA hybridization to dramatically increase the effective molarity of reactants linked to oligonucleotides, is a powerful strategy to control chemical reactivity in a DNA sequence-programmed manner.^{1–4} Because the reaction products of DTS are encoded by the sequences of the associated DNA templates, they can be subjected to in vitro selection followed by PCR amplification and DNA sequence analysis to enable the discovery of functional small molecules,^{3,5–7} synthetic polymers,^{8–10} or novel chemical reactions.^{11–15} We recently reported the three-step DNA-templated synthesis of a 13,824-membered small-molecule macrocycle library.¹⁶ The library was subjected to in vitro selection for binding affinity to a variety of proteins of biomedical interest, ultimately yielding a new class of macrocyclic kinase inhibitors.⁶ Other complementary approaches to generating DNA-encoded libraries have led to the discovery of bioactive small molecules,^{17–29} including a number of examples in the pharmaceutical industry.^{5,30,31}

Generating DNA-encoded small molecules of significant structural complexity requires multistep DNA-programmed or DNA-tagged synthesis.^{3,5,23,30,32–37} A number of strategies have been developed to enable multistep DTS. The simplest uses a DNA template strand containing several codons and reagents linked to complementary anticodon oligonucleotides that are added successively.^{3,32–34} While this approach is conceptually straightforward, it requires several manipulations after each step that increase required time and effort and can decrease overall yields. The relative geometry between reactants on the template and reagent strands also changes after each step in this approach, potentially altering reaction efficiencies.³⁸ More complex self-assembled DNA structures and devices can also mediate multistep DTS. For example, a DNA three-way junction that contains multiple reagents at the junction has been developed for the construction of DNA-encoded peptides.⁵ We developed a DNA mechanical device that moves along a DNA track and mediates autonomous multistep organic synthesis in a single isothermal solution.³⁵ McKee et al. recently used a DNA strand-exchange strategy to achieve a three-step DTS in which products are

swapped between new and old DNA strands with the assistance of a “remover strand” that displaces expended reagent oligonucleotides.³⁶

Despite these significant advances and the diversity of approaches to generating multistep DTS products, all multistep DNA-templated small-molecules syntheses reported to date have used only three or fewer DNA-templated steps, and overall yields are generally low (typically <10%). Here we present a new strand-displacement strategy for multistep DTS and its use to mediate a six-step synthesis with an overall yield of 35% (average yield of 83%). By providing products of six-step DNA-programmed reaction sequences in good overall yield, the approach presented here may provide access to high-complexity DNA-templated small-molecule libraries.

Our strategy exploits “toehold displacement,” the known ability of a single-stranded DNA oligonucleotide (AB) to invade an asymmetric DNA duplex (A'B':B) that contains a single-stranded hybridization site (A') for the invading strand.³⁹ Once A:A' hybridization takes place, base pairing with the invading strand continues, ultimately resulting in strand displacement of the shorter, and therefore less-favorably hybridized, B strand. Displacement results in the formation of a new Watson–Crick complex suitable for DTS. We hypothesized that this approach could represent a highly efficient and very simple way to access products of several consecutive DNA-programmed reactions while preserving the correspondence between DNA sequence and reaction product structure that is required for in vitro selection.

The application of this “toehold displacement” strategy to multistep DTS is summarized in Figure 1. A single-stranded DNA template (T) consists of a 16-base initial reaction site (black) followed by five consecutive 8-base coding segments (colored) that also serve as toeholds to initiate sequential DNA strand displacement. In the first step, substrate DNA S1, which is tethered to the first reactant, hybridizes to T, initiating DTS. If self-cleaving reagents are used, the first reactant group is transferred from S1 to T as a natural consequence of the DNA-templated reaction. After sufficient time to react has elapsed, the second substrate strand S2 is added without requiring product purification or any other manipulation. S2 partially hybridizes with T through the red toehold region and displaces S1 by forming a more stable DNA duplex due to the fact that the oligonucleotide in S2 is eight nucleotides longer than that in S1. As a result, S1 spontaneously leaves the Watson–Crick complex and the second reactant's group is transferred to the T-linked intermediate through a DNA-templated reaction. Thereafter, an

Received: February 13, 2011

Published: June 09, 2011

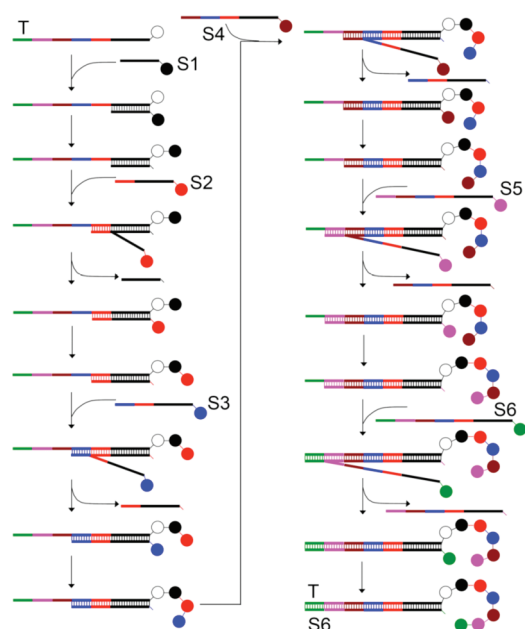


Figure 1. Toehold displacement—mediated multistep DNA-templated synthesis. In each step, hybridization between the template and substrate oligonucleotides triggers a DNA-templated reaction. The template strand contains multiple toehold regions (colored) that allow successive docking of new substrates and DNA strand displacement of oligonucleotides following each reaction without requiring purification after each step.

even longer substrate strand **S3** is added to displace **S2** and initiate a third reaction.

So long as unpaired toeholds (colored regions in Figure 1) remain in **T**, this process can be iterated to generate successively longer or more complex products without requiring any intervention during the reaction sequence beyond the simple addition of successive substrates to the same reaction vessel. Importantly, the effective molarity of the reactants during successive DNA-templated steps in this strategy remains relatively constant since the reactive groups for each step remain at the end of the double-stranded region.³⁸ As a result, we anticipated that reaction yields would remain higher over the course of many steps than with traditional multistep DTS methods. Crucially, the DNA templates in this strategy retain all product-encoding information throughout the DTS process, thus enabling the multistep products to be subjected to *in vitro* selections for desired properties, in contrast with a different approach to multistep synthesis that uses DNA strand exchange.³⁶

We designed and executed a six-step DNA-templated reaction sequence using this approach. The DNA template (**T**) contains a 3' primary amine group, and the first five substrates (**S1**–**S5**) contain 5' *N*-hydroxysuccinimide (NHS) ester-linked amines.^{32,35,37} The oligonucleotide–reagent bond is automatically cleaved as a result of the amine acylation reaction, thus enabling spontaneous transfer of the amino acid building block from each substrate to the template. The transferred amino acid displays another primary amine group that is poised to further react with the next NHS ester to continue the multistep DTS. The last substrate (**S6**) contains a biotin NHS ester and lacks a primary amine group (Figure 2).

In a typical experiment, **T** (1 μ M) and **S1** (1.2 μ M) were combined in aqueous buffer containing 50 mM MOPS and 10 mM Mg(OAc)₂ at pH 7.5. After 30 min at room temperature, the second substrate **S2** was added into the system, followed by another 30-min

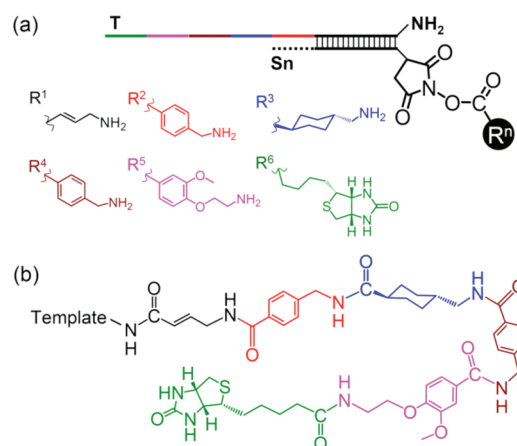


Figure 2. (a) Reactant structures; (b) expected six-step DNA-templated reaction product.

incubation at room temperature. Substrates **S3**–**S6** were similarly added at successive 30-min intervals. During the entire process, the temperature and buffer conditions were constant. The six-step reaction was therefore carried out in a single vessel at room temperature over 3 h. The crude reaction mixture was desalted by gel filtration and analyzed by high-resolution ESI mass spectrometry. For comparison, reactions containing only **T**, **T**+**S1**, **T**+**S1**+**S2**, **T**+**S1**+**S2**+**S3**, **T**+**S1**+**S2**+**S3**+**S4**, **T**+**S1**+**S2**+**S3**+**S4**+**S5**, and **S1**+**T**_{mis} (a template containing a scrambled DNA sequence) were also subjected to the reaction conditions and analyzed by high-resolution mass spectrometry.

The unreacted template and all six expected reaction products corresponding to one-, two-, three-, four-, five-, and six-step reaction sequences were observed with high mass accuracy (Figure 3). Each reaction resulted in highly efficient formation of the desired multistep product, such that the predominant template-linked ion observed from each reaction corresponded to the expected one- to six-step reaction product (Figure 3). The observation that in the six-step reaction mixture the template-linked full-length hexaamide product provided the strongest *m/z* signal among all template-linked ions suggested that the six-step product might be formed in excellent overall yield. The control reaction containing the mismatched template and **S1** did not generate detectable product (Figure 3), indicating that hybridization with the template is required to effect product formation under these conditions.

To quantitate reaction yields during all six reaction sequences, we used denaturing polyacrylamide gel electrophoresis (PAGE). Because each building block adds significant mass to the template, the full-length product and all the intermediate products migrate differently during PAGE. To achieve better separation during PAGE, all reaction products were digested with restriction endonuclease *DdeI*, which cleaves the 56-nt template into a 22-nt 3' fragment containing the reaction products. To enable accurate quantitation of reaction yields, a single fluorescein group was incorporated into the template (prior to DTS) near the 3' end, allowing the 22-nt fragments to fluoresce with equal intensity. Densitometry of fluorescein-visualized PAGE gel (Figure 4) revealed that the three-step reaction sequence (lane 4) generated the corresponding three-step product in 55% overall yield, and the six-step reaction sequence (lane 7) produced full-length hexaamide product in 35% overall yield, corresponding to ~83% average yield per step (see the Supporting Information [SI] for additional details). An independent experiment to determine reaction yields using nonfluorescein-labeled **T** in which

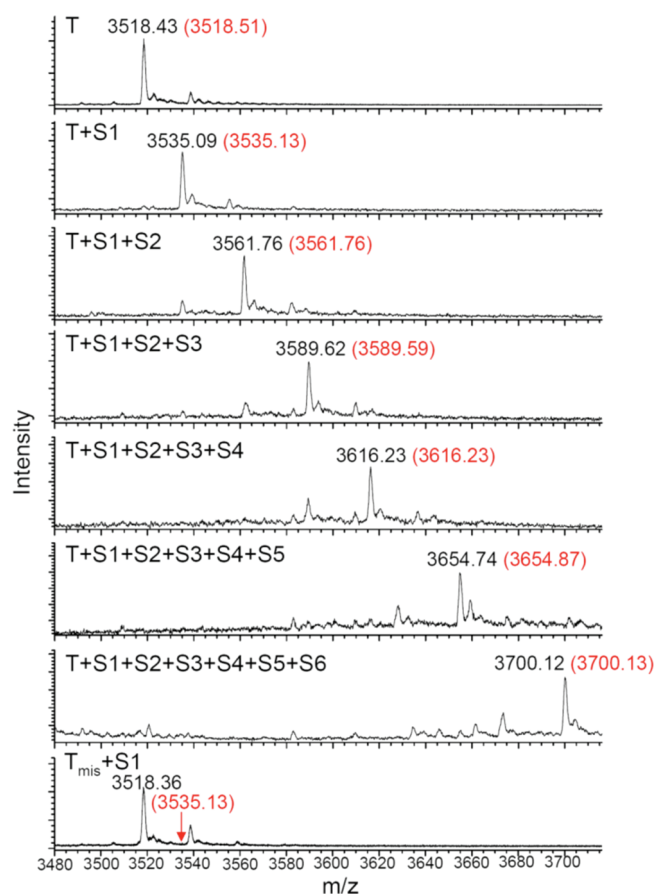


Figure 3. Mass spectrometric analysis of multistep DNA-templated reaction products generated by sequential strand displacement. Eight reactions using the species shown were separately performed as described in the text. The mass range shown includes all template-linked species. Observed m/z values for ions of -5 charge are shown in black; expected m/z values are shown in red. The arrow in the last spectrum indicates the expected m/z value of the product corresponding to reaction between S1 and a scrambled template (T_{mis}).

DdeI-digested reaction products were analyzed by PAGE followed by staining resulted in 38% overall yield of six-step reaction product (see the SI). To our knowledge, these results represent both the highest yielding and longest multistep DNA-templated small-molecule syntheses to date.^{32,35–37}

Applying this strategy for future multistep DNA-templated library syntheses will require that reagent-linked oligonucleotides each be prepared as mixtures containing all possible anticodons for prior DNA-encoded steps. The recent availability of inexpensive custom oligonucleotide pools from chip-based parallel synthesis^{40–43} provides practical access to these materials. In addition, the fact that the specificity-determining step of each reaction is hybridization of the 8-base toehold, which encodes the current reagent, implies that mismatch hybridization elsewhere in the template:reagent oligonucleotide duplex will not affect the fidelity of the multistep DTS process. Moreover, longer DNA templates could conceivably give rise to products of more than six DNA-programmed reactions. Indeed, we have observed that a 64-base, 80-base, and 96-base DNA strand in a duplex, sufficient to encode up to ~ 10 DNA-templated reactions, can be effectively displaced using a 72-mer, 88-mer, or 104-mer (see the SI and Figure S3).

lane	1	2	3	4	5	6	7	8
T	+	+	+	+	+	+	+	+
S1		+	+	+	+	+	+	
S2			+	+	+	+	+	
S3				+	+	+	+	
S4					+	+	+	
S5						+	+	
S6							+	

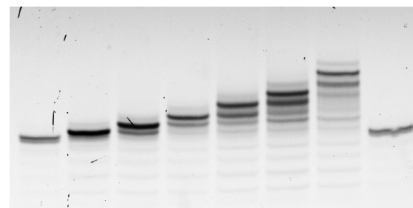


Figure 4. Denaturing PAGE analysis of the multistep DTS reactions analyzed in Figure 3. Each template-linked species contained a single fluorescein group to enable uniform visualization. The reaction products were digested with the endonuclease *DdeI* prior to PAGE analysis to cleave the product-linked oligonucleotides to 22-mers. Lanes 1 and 8: unreacted template; lanes 2–7: DNA template after successive reaction with one, two, three, four, five, or six reagents, respectively.

In summary, we developed a rapid, one-pot, highly efficient multistep DNA-templated synthesis strategy that is driven by successive toehold DNA strand displacement. The strategy was used to generate a six-step DTS reaction product in 35% overall yield (83% average yield per step), such that the desired product was the major observed template-linked species after six steps with no purification or reaction manipulation required beyond addition of each substrate every 30 min. Since the reaction history of the products remains encoded by their associate templates, this strategy may enable future efforts to generate high-complexity (e.g., n^6) DNA-templated libraries suitable for in vitro selection.

■ ASSOCIATED CONTENT

S Supporting Information. Complete ref 30, experimental methods, and additional experimental data. This material is available free of charge via the Internet at <http://pubs.acs.org>.

■ AUTHOR INFORMATION

Corresponding Author

drlu@fas.harvard.edu

■ ACKNOWLEDGMENT

This work was supported by the Howard Hughes Medical Institute and NIH/NIGMS (R01GM065865). We also thank Jia Niu for experimental assistance and David Gorin for helpful discussions.

■ REFERENCES

- (1) Gartner, Z. J.; Liu, D. R. *J. Am. Chem. Soc.* **2001**, *123*, 6961–6963.
- (2) Gartner, Z. J.; Kanan, M. W.; Liu, D. R. *Angew. Chem., Int. Ed.* **2002**, *41*, 1796–1800.
- (3) Gartner, Z. J.; Tse, B. N.; Grubina, R.; Doyon, J. B.; Snyder, T. M.; Liu, D. R. *Science* **2004**, *305*, 1601–1605.
- (4) Li, X. Y.; Liu, D. R. *Angew. Chem., Int. Ed.* **2004**, *43*, 4848–4870.

- (5) Hansen, M. H.; Blakskjaer, P.; Petersen, L. K.; Hansen, T. H.; Højfeldt, J. W.; Gothelf, K. V.; Hansen, N. J. *J. Am. Chem. Soc.* **2009**, *131*, 1322–1327.
- (6) Kleiner, R. E.; Dumelin, C. E.; Tiu, G. C.; Sakurai, K.; Liu, D. R. *J. Am. Chem. Soc.* **2010**, *132*, 11779–11791.
- (7) Silverman, S. K. *Angew. Chem., Int. Ed.* **2010**, *49*, 7180–7201.
- (8) Kleiner, R. E.; Brudno, Y.; Birnbaum, M. E.; Liu, D. R. *J. Am. Chem. Soc.* **2008**, *130*, 4646–4659.
- (9) Rosenbaum, D. M.; Liu, D. R. *J. Am. Chem. Soc.* **2003**, *125*, 13924–13925.
- (10) Brudno, Y.; Birnbaum, M. E.; Kleiner, R. E.; Liu, D. R. *Nat. Chem. Biol.* **2010**, *6*, 148–155.
- (11) Kanan, M. W.; Rozenman, M. M.; Sakurai, K.; Snyder, T. M.; Liu, D. R. *Nature* **2004**, *431*, 545–549.
- (12) Rozenman, M. M.; Kanan, M. W.; Liu, D. R. *J. Am. Chem. Soc.* **2007**, *129*, 14933–14938.
- (13) Momiyama, N.; Kanan, M. W.; Liu, D. R. *J. Am. Chem. Soc.* **2007**, *129*, 2230–2231.
- (14) Chen, Y.; Kamlet, A. S.; Steinman, J. B.; Liu, D. R. *Nat. Chem.* **2011**, *3*, 146–153.
- (15) Gorin, D. J.; Kamlet, A. S.; Liu, D. R. *J. Am. Chem. Soc.* **2009**, *131*, 9189–9191.
- (16) Tse, B. N.; Snyder, T. M.; Shen, Y. H.; Liu, D. R. *J. Am. Chem. Soc.* **2008**, *130*, 15611–15626.
- (17) Dumelin, C. E.; Scheuermann, J.; Melkko, S.; Neri, D. *Bioconjugate Chem.* **2006**, *17*, 366–370.
- (18) Halpin, D. R.; Harbury, P. B. *PLoS Biol.* **2004**, *2*, 1015–1021.
- (19) Halpin, D. R.; Harbury, P. B. *PLoS Biol.* **2004**, *2*, 1022–1030.
- (20) Halpin, D. R.; Lee, J. A.; Wrenn, S. J.; Harbury, P. B. *PLoS Biol.* **2004**, *2*, 1031–1038.
- (21) Melkko, S.; Zhang, Y.; Dumelin, C. E.; Scheuermann, J.; Neri, D. *Angew. Chem., Int. Ed.* **2007**, *46*, 4671–4674.
- (22) Melkko, S.; Mannocci, L.; Dumelin, C. E.; Villa, A.; Sommariva, R.; Zhang, Y. X.; Grutter, M. G.; Keller, N.; Jermutus, L.; Jackson, R. H.; Scheuermann, J.; Neri, D. *ChemMedChem* **2010**, *5*, 584–590.
- (23) Melkko, S.; Scheuermann, J.; Dumelin, C. E.; Neri, D. *Nat. Biotechnol.* **2004**, *22*, 568–574.
- (24) Scheuermann, J.; Dumelin, C. E.; Melkko, S.; Zhang, Y. X.; Mannocci, L.; Jaggi, M.; Sobek, J.; Neri, D. *Bioconjugate Chem.* **2008**, *19*, 778–785.
- (25) Mannocci, L.; Melkko, S.; Buller, F.; Molnar, L.; Bianke, J. P. G.; Dumelin, C. E.; Scheuermann, J.; Neri, D. *Bioconjugate Chem.* **2010**, *21*, 1836–1841.
- (26) Buller, F.; Steiner, M.; Scheuermann, J.; Mannocci, L.; Nissen, I.; Kohler, M.; Beisel, C.; Neri, D. *Bioorg. Med. Chem. Lett.* **2010**, *20*, 4188–4192.
- (27) Buller, F.; Zhang, Y. X.; Scheuermann, J.; Schafer, J.; Buhlmann, P.; Neri, D. *Chem. Biol.* **2009**, *16*, 1075–1086.
- (28) Mannocci, L.; Zhang, Y. X.; Scheuermann, J.; Leimbacher, M.; De Bellis, G.; Rizzi, E.; Dumelin, C.; Melkko, S.; Neri, D. *Proc. Natl. Acad. Sci. U.S.A.* **2008**, *105*, 17670–17675.
- (29) Wrenn, S. J.; Harbury, P. B. *Annu. Rev. Biochem.* **2007**, *76*, 331–349.
- (30) Clark, M. A.; et al. *Nat. Chem. Biol.* **2009**, *5*, 647–654.
- (31) Driggers, E. M.; Favaloro, F.; Li, X.; Li, G.; Benton, B.; Fraley, A.; Bittker, J.; Morales, A.; Harbeson, S.; Coull, J. 232nd ACS National Meeting, San Francisco, CA, United States, Sept. 10–14, 2006, pp 10–14.
- (32) Gartner, Z. J.; Kanan, M. W.; Liu, D. R. *J. Am. Chem. Soc.* **2002**, *124*, 10304–10306.
- (33) Li, X. Y.; Gartner, Z. J.; Tse, B. N.; Liu, D. R. *J. Am. Chem. Soc.* **2004**, *126*, 5090–5092.
- (34) Calderone, C. T.; Liu, D. R. *Angew. Chem., Int. Ed.* **2005**, *44*, 7383–7386.
- (35) He, Y.; Liu, D. R. *Nat. Nanotechnol.* **2010**, *5*, 778–782.
- (36) McKee, M. L.; Milnes, P. J.; Bath, J.; Stulz, E.; Turberfield, A. J.; O'Reilly, R. K. *Angew. Chem., Int. Ed.* **2010**, *49*, 7948–7951.
- (37) Snyder, T. M.; Liu, D. R. *Angew. Chem., Int. Ed.* **2005**, *44*, 7379–7382.
- (38) Gartner, Z. J.; Grubina, R.; Calderone, C. T.; Liu, D. R. *Angew. Chem., Int. Ed.* **2003**, *42*, 1370–1375.
- (39) Green, C.; Tibbetts, C. *Nucleic Acids Res.* **1981**, *9*, 1905–1918.
- (40) Tian, J. D.; Gong, H.; Sheng, N. J.; Zhou, X. C.; Gulari, E.; Gao, X. L.; Church, G. *Nature* **2004**, *432*, 1050–1054.
- (41) Lee, C. C.; Snyder, T. M.; Quake, S. R. *Nucleic Acids Res.* **2010**, *38*, 2514–2521.
- (42) Tian, J. D.; Ma, K. S.; Saaem, I. *Mol. Biosyst.* **2009**, *5*, 714–722.
- (43) Saaem, I.; Ma, K. S.; Marchi, A. N.; LaBean, T. H.; Tian, J. D. *ACS Appl. Mater. Interfaces* **2010**, *2*, 491–497.